SANDIA REPORT
SAND2013-0213
Unlimited Release
January 2013

Formation of Algae Growth Constitutive Relations for Improved Algae Modeling

Patricia E. Gharagozloo and Jessica L. Drewry

Prepared by
Sandia National Laboratories
Albuquerque, New Mexico 87185 and Livermore, California 94550

Sandia National Laboratories is a multi-program laboratory managed and operated by Sandia Corporation, a wholly owned subsidiary of Lockheed Martin Corporation, for the U.S. Department of Energy's National Nuclear Security Administration under contract DE-AC04-94AL85000.

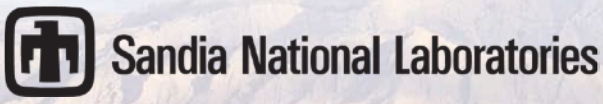

Issued by Sandia National Laboratories, operated for the United States Department of Energy by Sandia Corporation.

Available to DOE and DOE contractors from
U.S. Department of Energy
Office of Scientific and Technical Information
P.O. Box 62
Oak Ridge, TN 37831

Telephone: (865) 576-8401
Facsimile: (865) 576-5728
E-Mail: reports@adonis.osti.gov
Online ordering: http://www.osti.gov/bridge

Available to the public from
U.S. Department of Commerce
National Technical Information Service
5285 Port Royal Rd.
Springfield, VA 22161

Telephone: (800) 553-6847
Facsimile: (703) 605-6900
E-Mail: orders@ntis.fedworld.gov
Online order: http://www.ntis.gov/help/ordermethods.asp?loc=7-4-0#online

SAND2013-0213
Unlimited Release
January 2013

Formation of Algae Growth Constitutive Relations for Improved Algae Modeling

Patricia E. Gharagozloo and Jessica L. Drewry
Thermal/Fluid Science and Engineering
Sandia National Laboratories
MS9409
P.O. Box 969
Livermore, California 94551-0969

Abstract

This SAND report summarizes research conducted as a part of a two year Laboratory Directed Research and Development (LDRD) project to improve our abilities to model algal cultivation. Algae-based biofuels have generated much excitement due to their potentially large oil yield from relatively small land use and without interfering with the food or water supply. Algae mitigate atmospheric CO_2 through metabolism. Efficient production of algal biofuels could reduce dependence on foreign oil by providing a domestic renewable energy source. Important factors controlling algal productivity include temperature, nutrient concentrations, salinity, pH, and the light-to-biomass conversion rate. Computational models allow for inexpensive predictions of algae growth kinetics in these non-ideal conditions for various bioreactor sizes and geometries without the need for multiple expensive measurement setups. However, these models need to be calibrated for each algal strain. In this work, we conduct a parametric study of key marine algae strains and apply the findings to a computational model.

ACKNOWLEDGMENTS

The authors of this SAND report acknowledge the following people who provided additional assistance to enable the success of the project:

Todd Lane – guidance with lab-scale growth measurements
Pam Lane – guidance with lab-scale growth measurements
Scott James – guidance with EFDC and CE-QUAL models
Jerilyn Timlin – providing greenhouse and raceway data and general guidance
Ben Wu – program development
Neal Fornaciari – program development
Blake Simmons – program development
Greg Wagner – program support
Ryan Davis – *Dunaliella salina* guidance
Dave Brekke – help procuring lab space for lab-scale measurements
Aaron Collins – conducting greenhouse and absorptivity measurements
Howland Jones – absorptivity calculations
Kathy Alam – absorptivity measurements
Laura Martin – absorptivity measurements

CONTENTS

1. Introduction 9
   1.1. Background and Motivation 9
   1.2. Technical Approach 10
      1.2.1. Growth Model 10
      1.2.2. Growth Measurements 10

2. Growth Model 11
   2.1. Nutrients 11
   2.2. Light 12
   2.3. Temperature 13
   2.4. Salinity 13
   2.5. Conclusion 13

3. Growth Measurement 15
   3.1. Introduction 15
   3.2. Multi-factorial measurement 15
      3.2.1. Dunaliella salina 15
      3.2.2. Nannochloropsis salina 16
   3.3. Absorptivity measurement 17
   3.4. Conclusion 17

4. Emprical Parameter Calibration 19
   4.1. *Dunaliella salina* 19
      4.1.1. Nutrients 19
      4.1.2. Light 19
      4.1.3. Temperature 20
      4.1.4. Salinity 20
   4.2. *Nannochloropsis salina* 21
      4.2.1. Nutrients 21
      4.2.2. Light 21
      4.2.3. Temperature 21
      4.2.4. Salinity 22
   4.3. Conclusion 23

5. Model Validation 25
   5.1. Introduction 25
   5.2. Laboratory-scale 25
      5.2.1. Dunaliella salina 25
      5.2.3. Nannochloropsis salina 27
   5.3. Greenhouse ponds 30
   5.4. Open-channel Raceway 33
   5.5. Conclusion 35

6. Fluent Implementation 37
   6.1. Introduction 37
   6.2. CFD Model 37
   6.3. User Defined Functions 38

6.4. Fluent Model Verification 39
6.4.1. Example with known numerical solution 39
6.4.2. Greenhouse Model 40
6.5. Conclusion 44
7. Conclusions 45
8. References 47
Distribution (All electronic copy) 51

FIGURES

Figure 1. Plot of calibrated fluorescence data over time for three instances of a single *D. salina* growth case: 27 W/m^2, 1.0 M NaCl, and 26.5 °C. 16
Figure 2. Plot of calibrated fluorescence data over time for three instances of a single *N. salina* growth case: 27 W/m^2, 0.75 M NaCl, and 22 °C. 17
Figure 3. Plot of measured *D. salina* growth rates versus temperature for the measured NaCl concentrations at 27 W/m^2 with a sample calibration curve. 20
Figure 4. Plot of measured *D. salina* growth rates versus NaCl concentration for the measured light intensities at 26.5 °C with a sample calibration curve. 21
Figure 5. Plot of measured *N. salina* growth rates versus temperature for the measured NaCl concentrations at 27 W/m^2 with a sample calibration curve. 22
Figure 6. Plot of measured *N. salina* growth rates versus NaCl concentration for the measured light intensities at 26 °C with a sample calibration curve. 23
Figure 7. Plot of the predicted and measured *D. salina* concentration at laboratory scale over time at 26.5 °C and various light intensity and salinity conditions. 26
Figure 8. Plot of the predicted and measured *D. salina* concentration at laboratory scale over time at 29.5 °C and various light intensity and salinity conditions. 26
Figure 9. Plot of the predicted and measured *D. salina* concentration at laboratory scale over time at 31.5 °C and various light intensity and salinity conditions. 27
Figure 10. Plot of the predicted and measured *N. salina* concentration at laboratory scale over time at 18 °C and various light intensity and salinity conditions. 28
Figure 11. Plot of the predicted and measured *N. salina* concentration at laboratory scale over time at 22 °C and various light intensity and salinity conditions. 28
Figure 12. Plot of the predicted and measured *N. salina* concentration at laboratory scale over time at 26 °C and various light intensity and salinity conditions. 29
Figure 13. Plot of the predicted and measured *N. salina* concentration at laboratory scale over time at 30 °C and various light intensity and salinity conditions. 29
Figure 14. Plot of the light intensity and temperature over time for the greenhouse pond measurement. 30
Figure 15. Plot of the measured and predicted algae concentration over time for the greenhouse ponds. 31
Figure 16. Plot of the limitation factors over time for the greenhouse pond measurement. 32
Figure 17. Plot of the measured daily average and predicted instantaneous growth rates over time for the greenhouse ponds. 32

Figure 18. Plot of the light and temperature conditions over time for the open-channel raceway. 33
Figure 19. Plot of the measured and predicted algae concentration over time the open-channel raceway. 34
Figure 20. Plot of the limitation factors over time for the open-channel raceway. 34
Figure 21. Plot of the measured daily average and predicted instantaneous growth rates over time for the open-channel raceway. 35
Figure 22. Two-dimensional computational domain of the CFD model, 0.3 m deep by 1 m long. 37
Figure 23. Flow chart the interaction between the computational fluid dynamics (CFD) software and the user defined functions (UDF). 38
Figure 24. Chlorophyll-a and phosphorous concentration as a function of time for the Chapra problem. 40
Figure 25. Algae concentration as a function of time for the CFD, EFDC, and Runge Kutta models along with experimental data from a greenhouse experiment. 42
Figure 26. Carbon dioxide concentration as a function of time for the CFD, EFDC and Runge Kutta models without gas exchange with the surface. 42
Figure 27. Algae concentration as a function of time for the CFD, EFDC, and Runge Kutta models along with experimental data from a greenhouse experiment, assuming carbon dioxide transfer with the surface. 43
Figure 28. Carbon dioxide concentration as a function of time for the CFD, EFDC and Runge Kutta models without gas exchange with the surface. 43
Figure 29. Graph of the actual (xc) and saturation (xcsat) concentrations of carbon dioxide when algal growth is not present. 44

TABLES

Table 1. Initial and boundary for the Chapra problem. 39
Table 2. Greenhouse model parameters without exchange of carbon dioxide. 41

NOMENCLATURE

B	Biomass concentration (gC/m^3)
B_0	Initial biomass concentration (gC/m^3)
B_L	External biomass source or sink (gC/day)
B_M	Basal metabolic rate (1/day)
C	Carbon concentration (g/m^3)
C_0	Initial carbon concentration (g/m^3)
C_{chla}	Chlorophyll-a concentration (mg/L)
C_0	Initial chlorophyll-a concentration (mg/L)
CE-QUAL	U. S. Army Corp of Engineers' Water Quality Code
CFD	Computational Fluid Dynamics
CO_2	Carbon dioxide concentration (g/m^3)
DOE	Department of Energy
D. salina	*Dunaliella salina*
EFDC	Environmental Protection Agency's Environmental Fluid Dynamics Code
I	Light intensity (W/m^2)
I_0	Incident light intensity (W/m^2)
I_S	Optimal light intensity (W/m^2)
k_B	Background light extinction coefficient (m^2/gC)
k_c	Light extinction coefficient due to suspended biomass (or carbon) (m^2/gC)
k_{si}	Effect below (i = 1) or above (i = 2) optimal growth salinity (ppt^{-2})
K_i^T	Effect below (i = 1) or above (i = 2) optimal growth temperature ($°C^{-2}$)
$K_{OM,x}$	Rate organic nutrient (x) becomes available to algae (1/s)
K_X^h	Half-saturation constant for nutrient X (g/m^3)
N	Nitrogen concentration (g/m^3)
N_0	Initial nitrogen concentration (g/m^3)
N. salina	*Nannochloropsis salina*
NH_4	Ammonium concentration (gN/m^3)
NO_3	Nitrate concentration (gN/m^3)
P	Algae production (growth) rate (1/day)
P	Phosphorous concentration (g/m^3)
P_0	Initial phosphorous concentration (g/m^3)
PO_4	Phosphate concentration (gP/m^3)
P_R	Predation rate (1/day)
S	NaCl concentration (ppt or M)
S_{opt}	Optimal NaCl concentration (ppt or M)
SNL	Sandia National Laboratories
t	Time (days)
T	Temperature (°C)
T_i	Lower (i = 1) and upper (i = 2) optimal temperature (°C)
w_s	settling velocity (m/day)
μ	exponential growth rate (1/day)
ν	nutrient concentration (g/m^3)

1. INTRODUCTION

1.1. Background and Motivation

Typical methods for growing high lipid content algae stress the algae at non-ideal growth conditions causing them to store energy in the form of lipids. Algae growth through photosynthesis is dependent on light intensity, temperature, salinity, pH, and availability of nutrients [1]. Abiotic stress from variations in these conditions has been shown to affect lipid composition and quantities [2]. Modeling a wide range of culture conditions will reduce the need for large expensive measurements.

Light provides the energy for photosynthesis. At low luminescence levels, insufficient energy is available for growth while above optimal levels algae may become stressed and produce TAGs and experience photobleaching. Nutrients like CO_2, phosphate, sulfate, and nitrate play important roles in photosynthesis. Excess nutrients allow for high growth rates and production of nitrogen-containing chlorophyll and sulfur and phosphorous containing lipids. A nutrient shortage results in higher production of TAGs with reduced levels of chlorophyll and sulfur/phosphorous lipids.

The temperature range for ideal growth of each algae strain depends on its native habitat and can vary from the low temperatures of the arctic to the high temperatures of the desert. When temperatures deviate from ideal, growth rates diminish. Temperatures higher than ideal for growth tend to cause reduced lipid production while lower temperatures tend to increase lipid production (at low temperatures, algae produce more lipids to prevent membrane hardening) [1-3].

For freshwater algae, increasing salinity decreases the growth rates. For halophilic and halotolerant algae, ideal salinities typically depend on the algae's native habitat. At salinities above or below this value, growth rates decrease [4-9]. No consistent pattern has been seen with regard to salinity variation and lipid production in halophilic and halotolerant algae. Each type of algae seems to have an individualized response [10, 11]. However, limited data are available for this dependence.

Large-scale bioreactor systems needed for commercial scale biofuel production, whether open raceway ponds or closed photobioreactor systems, experience large variations in environmental conditions spatially and temporally over the course of a day, month or year. Light conditions vary due to typical diurnal and annual cycles, variations in cloud cover, the angle of the sun, and shading by other algae in the culture. The temperature of the culture depends on the thermal radiation from the sun, wind speed and temperature, and evaporation. Nutrients vary due to differing consumption and delivery rates. The pH depends on the carbon dioxide concentration as well as the algae's own pH regulatory mechanisms [12]. Salinity varies due to evaporation and rain fall. It is important for a computational model to be able to realistically model these systems for all potential environmental conditions. However, the wealth of data needed to populate a model for specific strains is not available. Additionally, the growth model has yet to be fully validated for cultivation systems.

The green algae *Dunaliella salina* can produce large quantities of lipids making it appealing for oil production [1]. It can be grown in extreme conditions including high salt, high pH, and high temperatures, which reduces the threat of contamination. *Dunaliella* strains are currently used for commercial production of β-carotene [13]. Although many researchers have studied *Dunaliella salina* [7, 14-27], no fully parametric data have been published on a single strain to facilitate development of a strain-specific computational model.

The green algae *Nannochloropsis salina*, has been observed as a potential biofuel production algae [10, 28]. It is a halo-tolerant species that can be grown in non-potable water. As with most algae strains, no fully parametric data has been published.

Traditional methods for growing algae parametrically and for measuring growth and lipid production are cumbersome. Most require large aliquots of dried algae. Our growth method will vary multiple parameters between samples in a given measurement period to reduce the time to complete the parametric study. The experimental methods will allow for in-situ measurements of growth rates reducing the amount of algae mass needed to be grown.

1.2. Technical Approach

This project addresses the short comings described in Section 1.1 through the development of *in vivo* multifactorial measurements to calibrate the model and by validating the calibrated model in multiple cultivation type bioreactors.

1.2.1. Growth Model

This work uses a modified version of the U. S. Army Corp of Engineers' water-quality code (CE-QUAL) [29, 30] to simulate algal growth kinetics in well-mixed photobioreactor-type systems. The model allows the flexibility to manipulate a host of variables associated with algal growth such as temperature, light intensity, and nutrient availability. Salinity of the medium is another important operational parameter governing algal growth; the effects of salinity are added to the model to expand its capabilities to marine algae. The effect of pH is not investigated in this study due to the desire to have consistent CO_2 levels for each of the conditions during the calibration. However, it is currently being implemented into CE-QUAL by James and Janardhanam [31].

1.2.2. Growth Measurements

To populate the model's algae specific empirical parameters, we conduct parametric growth-rate measurements of *Dunaliella salina* (*D. salina)* and *Nannochloropsis salina* (*N. salina*) at different temperatures, light intensities, and salinities.

2. GROWTH MODEL

The governing equation for algal biomass growth in CE-QUAL is [29]:

$$\frac{\partial B}{\partial t} = \left((P - B_M - P_R)\right)B + \frac{\partial}{\partial z}\left((w_s B)\right) + \frac{B_L}{V}, \quad (1)$$

where B (gC/m^3) is the biomass, t (days) is time, P (day^{-1}) is the production (growth) rate, B_M (day^{-1}) is the basal metabolic rate, P_R (day^{-1}) is the predation rate, w_s (m/day) is the settling velocity, B_L (gC/day) represent the external loads such as deposition or sources, and V (m^3) is the model cell volume. Biomass production rates are determined by the availability of nutrients (including CO_2), the intensity of light, local temperature, pH, and salinity. For this work we are adding in the effect of salinity and neglecting the effect of pH. The effect of each is considered to be multiplicative and decoupled [29]:

$$P = P_M f(n) g(I) h(T) i(S) j(pH). \quad (2)$$

Here, P_M is the maximum instantaneous growth rate under optimal conditions (day^{-1}), $f(v)$ is the effect of non-optimal nutrients, which includes CO_2 limitation ($0 \le f(v) \le 1$), $g(I)$ is the effect of non-optimal illumination ($0 \le g(I) \le 1$), $h(T)$ is the effect of non-optimal temperature ($0 \le h(T) \le 1$), $i(S)$ is the effect of non-optimal salinity ($0 \le i(S) \le 1$), and $j(pH)$ is the effect of non-optimal pH ($0 \le j(pH) \le 1$). All of these functions are spatially dependent, and their values vary from cell to cell in the model according to local nutrient concentrations (including CO_2), incident solar radiation, salinity and temperature. For this work, we are growing algae in well-mixed lab conditions. Additionally, for the initial validation study, we assume that the larger-scale systems are well mixed and controlled. Therefore, we neglect the effects of predation and settling. Future studies will address these components of the model.

2.1. Nutrients

Growth limitation due to nutrient availability is based on the Monod equation [32]:

$$f(n) = \frac{n}{K_X^h + n}, \quad (3)$$

where v (g/m^3) is the nutrient concentration and K_X^h is the half-saturation constant. For example, the nutrient function for green algae can be nutrient limited by dissolved ammonium, nitrate, phosphate, or CO_2, yielding:

$$f(n) = \min\left(\frac{NH_4 + NO_3}{K_N^h + NH_4 + NO_3}, \frac{PO_4}{K_P^h + PO_4}, \frac{CO_2}{K_C^h + CO_2}\right) \quad (4)$$

Here, NH_4 (gN/m^3) is the ammonium concentration, NO_3 (gN/m^3) is the nitrate concentration, PO_4 (gP/m^3) is the dissolved phosphate concentration, CO_2 (g/m^3) is the dissolved carbon dioxide concentration, and K_N^h, K_P^h, and K_C^h are the corresponding half-saturation constants.

2.2. Light

Algae production is a function of suboptimal light, which is a function of average daylight, light extinction, light intensity at the water surface, optimal light intensity, and depth of the algae below the water surface. Algae grow as the light intensity increases to some saturation (optimum) intensity (I_s) beyond which growth rates decline due to photo-inhibition. The function for non-optimal illumination is derived from Steele's equation [33, 34]:

$$g(I) = \frac{I(z)}{I_s} e^{1-\frac{I(z)}{I_s}}, \tag{5}$$

where $I(z)$ (W/m^2) is the instantaneous light intensity at depth z (m) and I_s (W/m^2) is the optimal light intensity. If the growth medium is not well-mixed, then the rate of change of light intensity $I(z)$ changes with depth (or model layer) due to non-uniform growth of algae. If, on the other hand, the system is well mixed, then the biomass concentration will be homogeneous (constant light extinction). For such a system (i.e., the single-layer model studied in this work), the growth limitation is:

$$g(I) = \frac{e}{K_e d}\left(\left(e^{-a_1} - e^{-a_0}\right)\right), \tag{6}$$

where d (m) is the water-layer depth, K_e (m^{-1}) is the light extinction coefficient, a_0 (−) is the light intensity ratio at the top of the water surface:

$$a_0 = \frac{I_0}{I_s}, \tag{7}$$

and a_1 (−), the ratio at the bottom (of the layer) is:

$$a_1 = \frac{I_0}{I_s} e^{-K_e d}. \tag{8}$$

Note that recursive calculations are necessary for multi-layer models.

The light extinction coefficient, K_e, in a single layer model and within a particular layer in a multi-layer hydrodynamics model is considered to be a constant and can be formulated as

$$K_e = k_B + k_c B, \tag{9}$$

where k_B (m^{-1}) is the constant background light extinction coefficient due to water and other suspended particulates and k_c $(gC/m^3)^{-1}/m$ is the constant light extinction due to suspended carbon (or biomass) concentration in the layer. A standard value of 0.1 m^{-1} is typically used for k_B.

2.3. Temperature

Algal growth rate increases with temperature up to an optimal and decreases with any further increase [35]. Temperature effects on each algae group are defined by an exponential function of water temperature, the optimal temperature for growth, and the temperature-effect coefficients below and above the optimal temperatures:

$$h(T) = \begin{cases} \exp\left[K_1^T((T - T_1))^2\right] & \text{for } T \le T_1 \\ 1 & \text{for } T_1 < T \le T_2 \\ \exp\left[K_2^T((T_2 - T))^2\right] & \text{for } T > T_2 \end{cases}, \qquad (10)$$

where T (°C) is the local temperature from the hydrodynamic model, T_1 (°C) is the lower optimal growth temperature, T_2 (°C) is the upper optimal growth temperature, K_1^T ($°C^{-2}$) is the temperature effect below the optimal growth temperature, and K_2^T ($°C^{-2}$) is the temperature effect above the optimal growth temperature of the algal group.

2.4. Salinity

Marine algae growth rates have an optimum salinity above and below which the growth rate decreases [5-9]. The salinity of the media is limited to a range between zero for a completely non-saline solution to its maximum solubility in water. The effect of salinity on algae growth has yet to be formulated into a general equation that can be applied to a variety of halotolerant/halophilic algae species. Given the similarity in curve shape to temperature, we propose an exponential function for salinity:

$$i(S) = \begin{cases} \exp\left(-k_{s1}(S - S_{opt})^2\right) & \text{for } S \le S_{opt} \\ \exp\left(-k_{s2}(S - S_{opt})^2\right) & \text{for } S > S_{opt} \end{cases}, \qquad (11)$$

where S (ppt) is the salinity, S_{opt} (ppt) is the optimal salinity, k_{s1} (ppt^{-2}) is the salinity effect below the optimal salinity, and k_{s2} (ppt^{-2}) is the salinity effect above the optimal salinity.

2.5. Conclusion

The CEQUAL growth model predicts algae growth by accounting for limitations in productivity due to non-optimal temperature, light intensity, salinity, nutrients, and pH. The model can be used to optimize pond design and strain selection. However, the model requires calibration for each potential algae strain.

3. GROWTH MEASUREMENT

3.1. Introduction

Traditional methods for growing algae parametrically and for measuring growth and lipid production are cumbersome. Most require large aliquots of dried algae. Our growth method will vary multiple parameters between samples in a given measurement period to reduce the time to complete the parametric study. The experimental methods will allow for in-situ measurements of growth rates reducing the amount of algae mass needed to be grown.

The green algae *Dunaliella salina* can produce large quantities of lipids making it appealing for oil production [1]. It can be grown in extreme conditions including high salt, high pH, and high temperatures, which reduces the threat of contamination. *Dunaliella* strains are currently used for commercial production of β-carotene [13]. Although many researchers have studied *D. salina* [7, 14-27], no fully parametric data have been published on a single strain to facilitate development of a strain-specific computational model. Another green algae, *Nannochloropsis salina*, has also been observed as a potential biofuel production algae [10, 28]. It is a halo-tolerant species that can be grown in non-potable water. As with most algae strains, no fully parametric data has been published.

3.2. Multi-factorial measurement

Dunaliella salina 1644 from UTEX is grown in 2x Erdschreiber's medium. *Nannochloropsis salina* CCMP 1776 is grown in F/2 medium. The cultures are adapted to light conditions, NaCl concentrations, and temperatures. The cultures are grown in 25 mm test tubes with air bubbled through a plastic tube submerged to the bottom of the test tube to provide CO_2 and mixing. The diurnal cycles are set at 16:8 and the temperature is held constant for each measurement set. A calibrated digital fluorometer (Turner Designs/10-AU) measures the chlorophyll a fluorescence *in vivo*. The fluorescence is calibrated with known chlorophyll standards. The measurements are calibrated to initial culture cell counts. The fluorescence is measured daily to produce growth curves for each of the sets of conditions.

The fluorometer transmits an excitation beam of light in the 440nm range and detects light emitted from the sample in the 680nm range. Although chlorophyll fluorescence is not an appropriate method for measuring a quantitative chlorophyll a concentration, the change in fluorescence over time of a given sample can be used as an efficient method to calculate the rate of change of the sample concentration or growth rate.

3.2.1. Dunaliella salina

Growth rates for *D. salina are* calculated from data measured in triplicate at three light conditions (10.5, 27, and 58 W/m^2), four NaCl concentrations (1, 1.5, 2 and 2.5M), and four temperatures (23.5, 26.5, 29.5, 31.5°C). The concentration over time during the exponential growth phase is represented by the equation $C_{Chla}(t) = C_0 \exp(\mu t)$, where C_{chla} is the chlorophyll a concentration, C_0 is the initial chlorophyll-a concentration, t is the time, and μ is the exponential growth rate. The growth rates are calculated by linear curve fits to data from the

exponential growth phase to $\ln(C_{Chla}) = \mu t + \ln(C_0)$ and averaged over the triplicate samples for each growth condition. A sample set of data at a specific growth condition with a light intensity of 27 W/m^2, NaCl concentration of 1.0M, and a temperature of 26.5°C is shown in Figure 1.

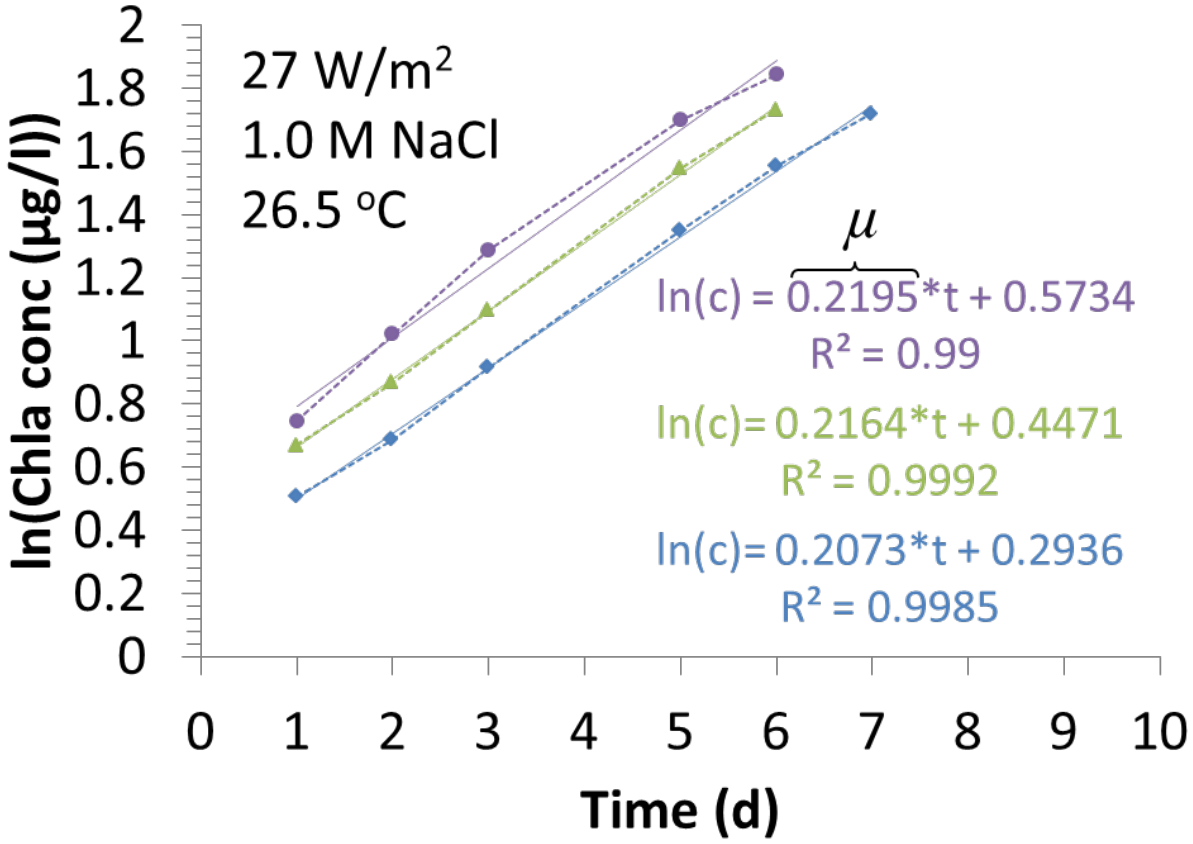

Figure 1. Plot of calibrated fluorescence data over time for three instances of a single *D. salina* growth case: 27 W/m^2, 1.0 M NaCl, and 26.5 °C.

3.2.2. Nannochloropsis salina

Growth rates for *N. salina* are calculated from data measured in triplicate at three light conditions (10.5, 27, and 58 W/m^2), four NaCl concentrations (0.35, 0.5, 0.75 and 1M), and four temperatures (18, 22, 26, 30°C). The concentration over time during the exponential growth phase is represented by the equation $C_{Chla}(t) = C_0 \exp(\mu t)$, where C_{chla} is the chlorophyll a concentration, C_0 is the initial chlorophyll-a concentration, t is the time, and μ is the exponential growth rate. The growth rates are calculated by linear curve fits to data from the exponential growth phase to $\ln(C_{Chla}) = \mu t + \ln(C_0)$ and averaged over the triplicate samples for each growth condition. A sample set of data at a specific growth condition with a light intensity of 27 W/m^2, NaCl concentration of 0.75M, and a temperature of 22°C is shown in Figure 2.

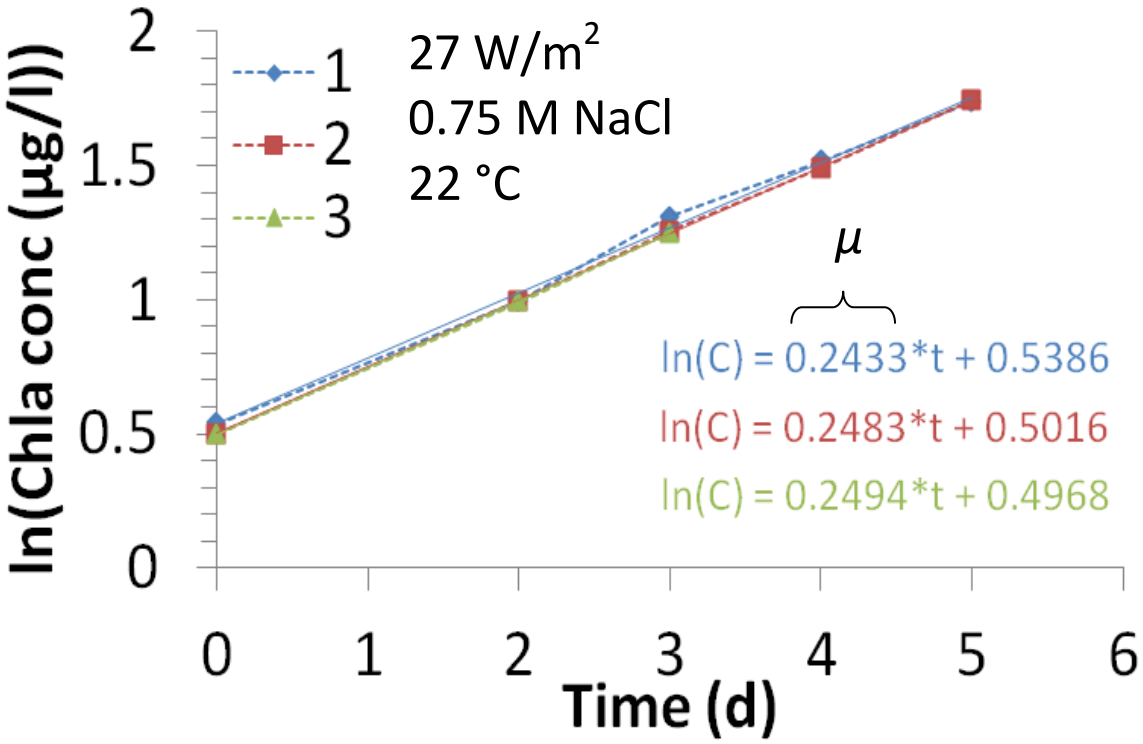

Figure 2. Plot of calibrated fluorescence data over time for three instances of a single *N. salina* growth case: 27 W/m^2, 0.75 M NaCl, and 22 °C.

3.3. Absorptivity measurement

3.4. Conclusion

Multifactorial measurements were conducted on *D. salina* and *N. salina*. These measurements have been used to calculate growth rates for a range of environmental parameters. In the following section the measured growth rates will be used to calibrate the algae specific empirical parameters in the computation model.

4. EMPIRICAL PARAMETER CALIBRATION

Each strain of algae has evolved to grow in the conditions of their native habitat. Given the large variations in environmental conditions between seasons and locations, significant difference exist between the various algae strains in the growth response to environmental conditions. This results in the model requiring calibration for each strain of interest. However, it also allows the model to be used to devise an ideal strain for particular locations and seasons to set as an engineering or prospecting goal.

While many parameters that the model is sensitive to are also highly variable between strains and sensitive, others either vary little between strains or do not substantially affect the model. These are typically set to standard values for green algae. For instance, the basal metabolism rate is set to 0.01 1/d [36]. Nutrients recycle in the system as algae metabolize the inorganic forms of nitrate and phosphate into their dissolved organic forms. These dissolved organic nitrates and phosphates are mineralized back into their inorganic forms at rates of 0.015 and 0.1 day^{-1} [29]. All of these water-quality variables are tracked in the model.

Half-saturation constants are typically defined for the low concentrations of nutrients common in environmental systems and are on the order of 0.01 g/m^3. For algal growth systems (bioreactors), nutrients are often added in excess and the nutrient limiting function is close to unity. However, CO_2 is often difficult to maintain at high enough concentrations particularly during high growth periods, in large reactors, and at high algae concentrations. Also, when algae are nutrient deprived (e.g., to trigger lipid production), the value of the half-saturation constant will play a more important role in algae growth.

4.1. *Dunaliella salina*

4.1.1. Nutrients

For the calibration of *D. salina*, we ensure that the nutrients are always well in excess of the half saturation constants so that algae are not nutrient limited. Because the exact values for the half saturation constants are not important when in significant excess, the default values in CE-QUAL are used (K_N^h = 0.01 g/m^3, K_P^h = 0.002 g/m^3, and K_C^h = 0.05 g/m^3). The nutrient consumption rate is based on the Redfield C:N:P ratio of 106:16:1 [37]. If the cultivation is expected to be run in nutrient limiting conditions, these values would need to be updated to ensure nutrients are consumed at the appropriate rate and growth is limited at low nutrient concentrations.

4.1.2. Light

To model *Dunaliella salina*, the light extinction value is found from literature. A value of 0.017 $(gC/m^3)^{-1}/m$ is used for k_c [14]. The optimal light intensity was calibrated from the growth rate data. The optimal light intensity for *D. salina* is found to be 31 W/m^2.

4.1.3. Temperature

A plot of the measured growth rates versus temperature for various salinities at a light intensity of 27 W/m^2 is shown in Figure 3 along with a calibration curve. The fitted lower and upper optimal growth temperatures are 27°C and 28°C, respectively. The fitted temperature effects below and above optimal are 0.02 °C^{-2} and 0.025 °C^{-2}, respectively.

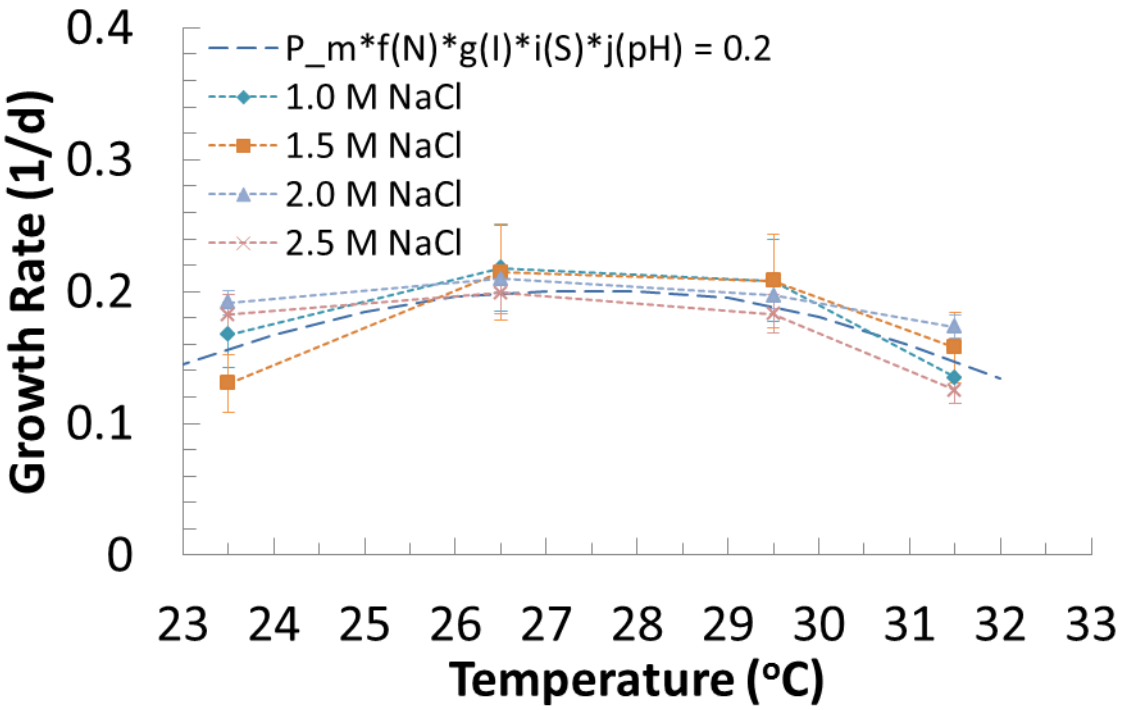

Figure 3. Plot of measured *D. salina* growth rates versus temperature for the measured NaCl concentrations at 27 W/m^2 with a sample calibration curve.

4.1.4. Salinity

The measured growth rates as a function of NaCl concentration for various light intensities at a temperature of 26.5 °C are plotted in Figure 4 along with model calibration curves. The fitted optimal NaCl concentration is 90 ppt or 1.54 M and the fitted salinity effect below and above optimal is 5e-5 ppt^{-2} and 6e-5 ppt^{-2}, respectively. The optimal NaCl concentration is high and the exponential constants are small due to the highly halophilic nature of *Dunaliella salina*.

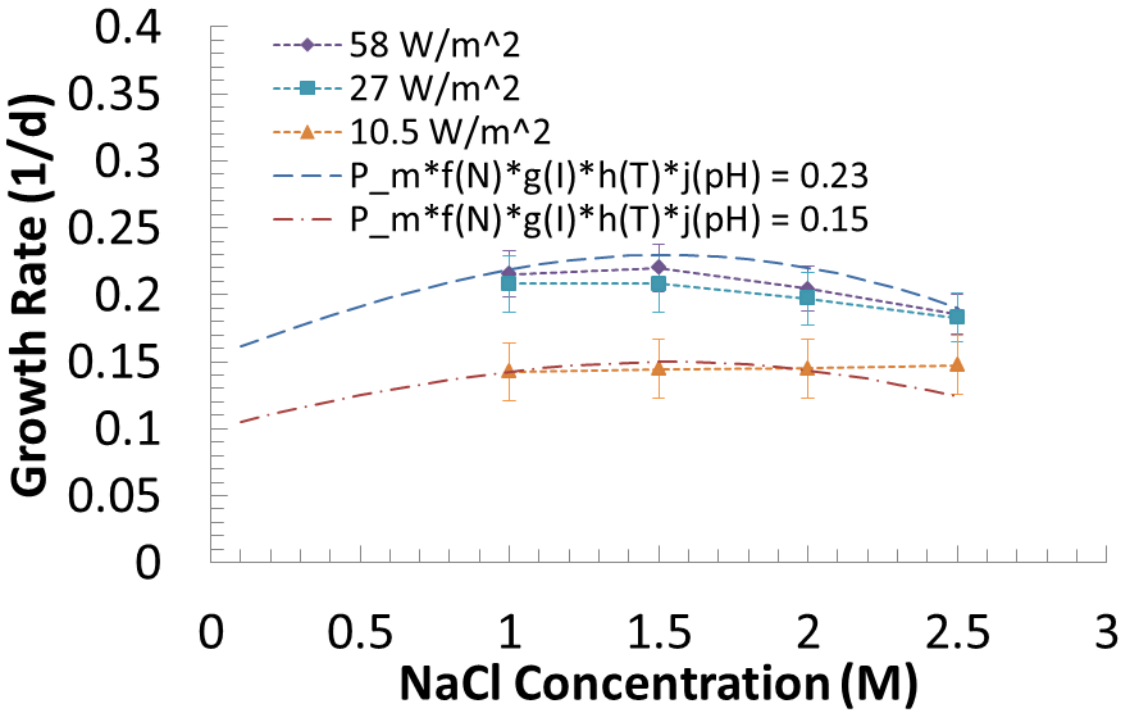

Figure 4. Plot of measured *D. salina* growth rates versus NaCl concentration for the measured light intensities at 26.5 °C with a sample calibration curve.

4.2. *Nannochloropsis salina*

4.2.1. Nutrients

The half-saturation constants used in this model are 0.01 g/m^3 [36], 0.002 g/m^3 [36], and 0.028 g/m^3 [38] for nitrogen, phosphorous, and CO_2 respectively. Algae atomic composition ratios were measured for *N. salina* three times over the course of the experiment. Samples were collected on days 7, 11, and 14 of the greenhouse growth experiment yielding C:N:P ratios of 358:38:1, 365:36:1, and 423:39:1, respectively (for reference, the Redfield ratio for marine planktons in open oceans is 106:16:1 [37]). Significant variability of elemental composition exists across strains and even within strains due to environmental stressors and adaptations. A C:N:P ratio of 358:38:1 was applied for *N. salina* in the simulations.

4.2.2. Light

To model *Nannochloropsis salina*, the light extinction coefficient, k_c, measured in the absorptivity measurement discussed in Section 2.3, is found to be 0.2856 m^2/gC. The optimal light intensity, I_s, was fit to the lab-scale growth rate data. The optimal light intensity is determined to be 20 W/m^2.

4.2.3. Temperature

A plot of the measured growth rates versus temperature for various salinities at a light intensity of 27 W/m^2 is shown in Figure 5 along with results for the fitted constitutive relation. The fitted lower and upper optimal growth temperatures are 21.5°C and 23.5°C, respectively. The fitted temperature effects below and above optimal are 0.015 and 0.01, respectively.

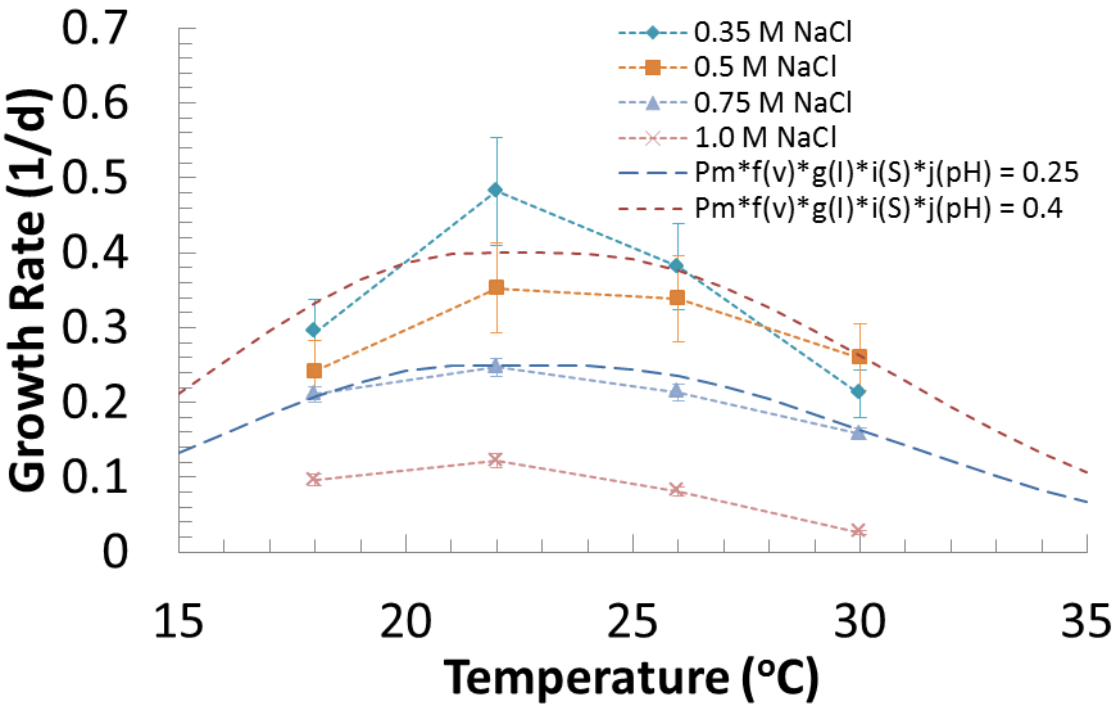

Figure 5. Plot of measured *N. salina* growth rates versus temperature for the measured NaCl concentrations at 27 W/m^2 with a sample calibration curve.

4.2.4. Salinity

The measured growth rates as a function of NaCl concentration for various light intensities 26°C are plotted in Figure 6 along with model predictions for different conditions for temperature and light intensity. The fitted optimal NaCl concentration is 20 ppt or 0.35 M and the fitted salinity effect above optimal is 9e-4 ppt^{-2}, we did not measure salinities below the optimal value since the starting media was at approximately the optimal salinity. Thus, the effect below optimal is assumed to be the same as above optimal.

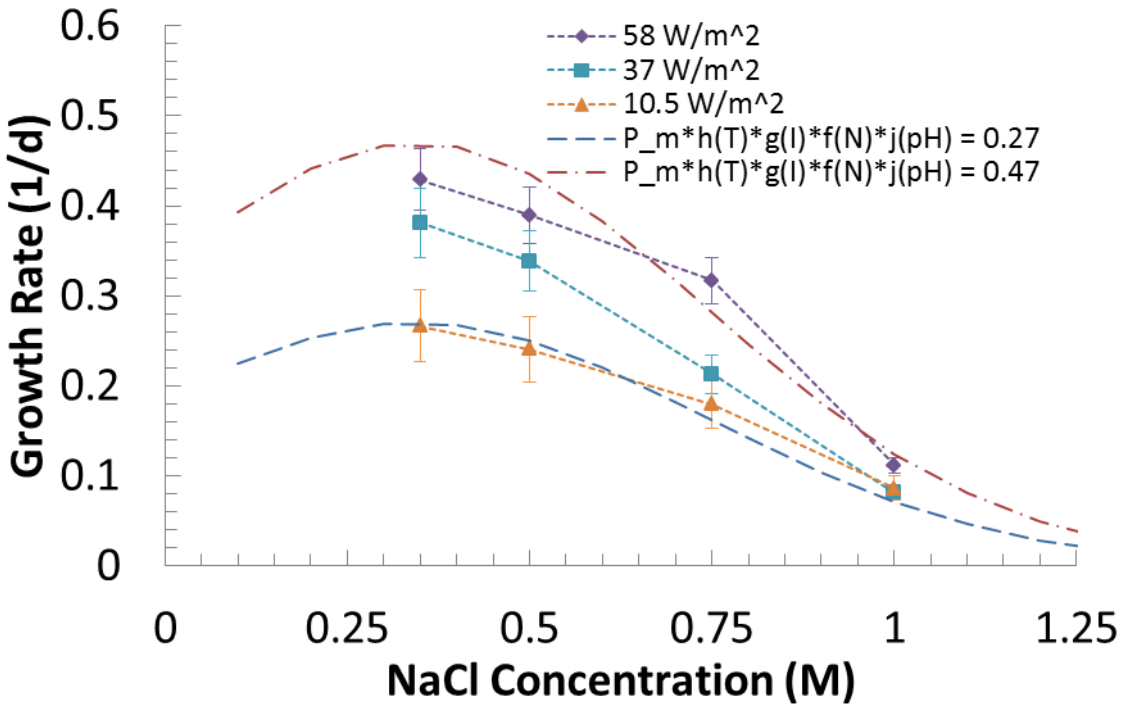

Figure 6. Plot of measured *N. salina* growth rates versus NaCl concentration for the measured light intensities at 26 °C with a sample calibration curve.

4.3. Conclusion

The model's empirical parameters have been calibrated for two potential lipid producing algae strains. These calibrations can now be used to validate the model by comparing to growth measurements. The following section will discuss this model validation.

5. MODEL VALIDATION

5.1. Introduction

Before applying a model to optimize commercial systems, it is necessary conduct a validation and ensures the model can appropriately predict growth response in a variety of conditions. For *D. salina*, the calibrated model is applied to the laboratory-scale measurements used in the model calibration. Although not a full validation, the comparison gives a sanity check that the calibration and model are giving realistic results. For *N. salina*, the calibrated model is also applied to the laboratory-scale measurements used in the model calibration. Then, to validate the model, the calibrated model is applied to two additional measurements: greenhouse ponds and an open-channel raceway.

5.2. Laboratory-scale

The developed empirical fits are now supplied to the model and compared with the measurements. The model is set up for a completely mixed 15 x 2.2 x 2.2 cm^3 rectangular culture volume to represent the test tubes used in the experiments (equivalent volume). The modeled test tube is exposed to light from one side at the specified intensities.

5.2.1. Dunaliella salina

The model includes the initial nutrient concentrations for the 2X Erdschreiber's medium of 2.3 mM NO_3 (32.2 gN/m^3) and 0.067 mM PO_4 (2.075 gP/m^3). The CO_2 is set initially to 0.9 g/m^3 [39]. The absorption of CO_2 into the media from the bubbling of air is assumed to be much more than sufficient to sustain this amount of CO_2 (2.31 µg/s). The initial algae concentrations are specified to match the initial measured concentrations.

Figure 7 – Figure 9 show the algae concentrations from measurements and simulation over time at temperatures of 26.5 °C, 29.5 °C, and 31.5 °C, respectively, and various light intensities and NaCl concentrations. For the most part, the data fit well to the calibrated model.

For the best fit between the model and measurements, the ideal growth conductions for *D. salina* are determined to be a NaCl concentration of 1.54 M, a light intensity of 31 W/m^2, and a temperature between 27 and 28 °C. The maximum measured daily average growth rate in this study is 0.27 1/d, which when divided by 2/3 for the fraction of the day with light gives 0.4 1/d as the maximum instantaneous growth rate. The theoretical maximum productivity, P_M, used in equation (2) is determined to be 2.5 1/d. The typical trends were observed, the growth rate diminished at temperatures and salinities above and below the optimal value. The growth rate also diminished at light intensities below the optimal intensity and leveled out at higher intensities. Although slight pigment change was observed at the highest light intensity, we did not observe a decrease in growth rate.

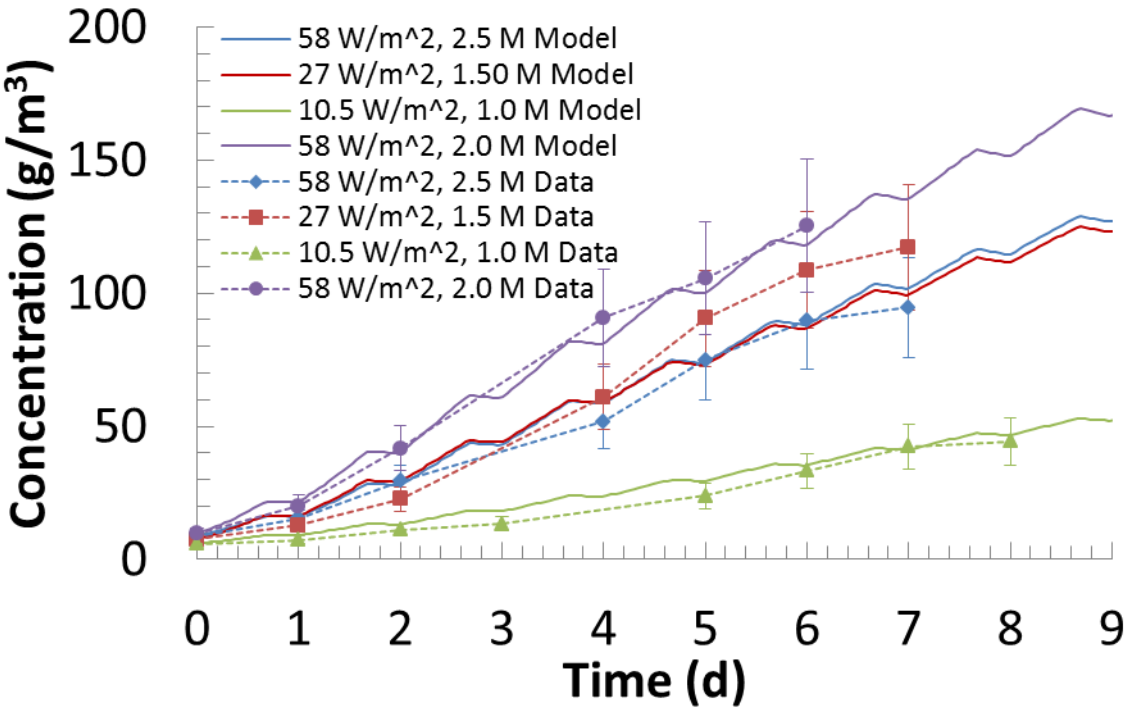

Figure 7. Plot of the predicted and measured *D. salina* concentration at laboratory scale over time at 26.5 °C and various light intensity and salinity conditions.

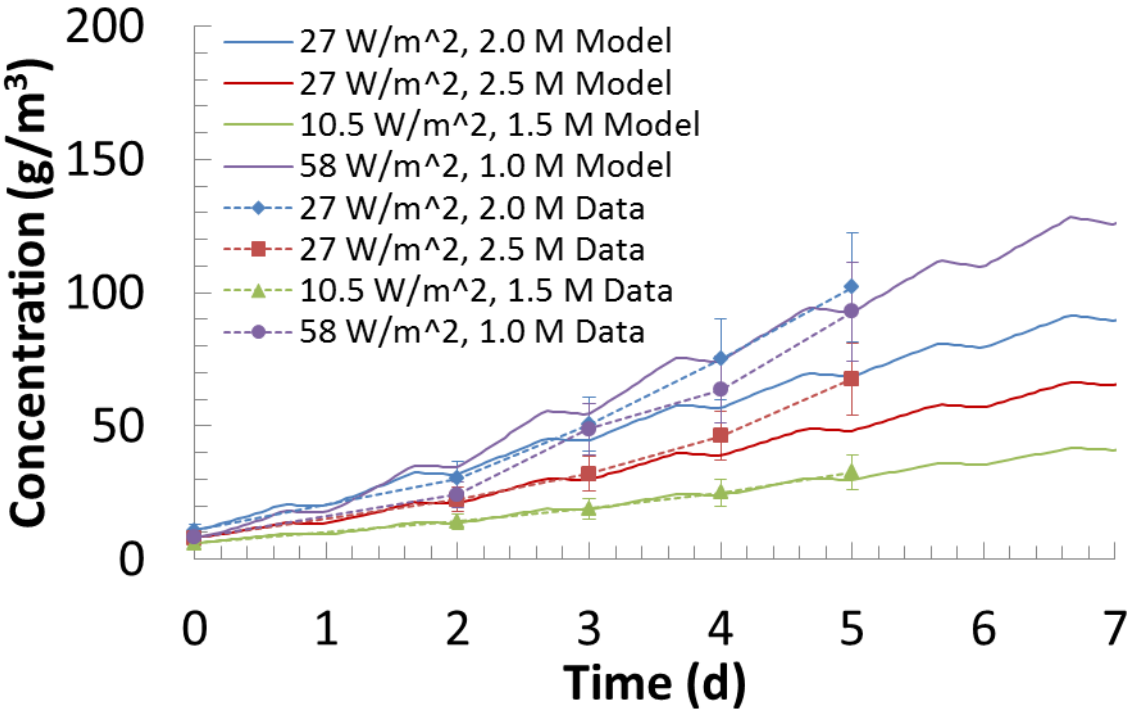

Figure 8. Plot of the predicted and measured *D. salina* concentration at laboratory scale over time at 29.5 °C and various light intensity and salinity conditions.

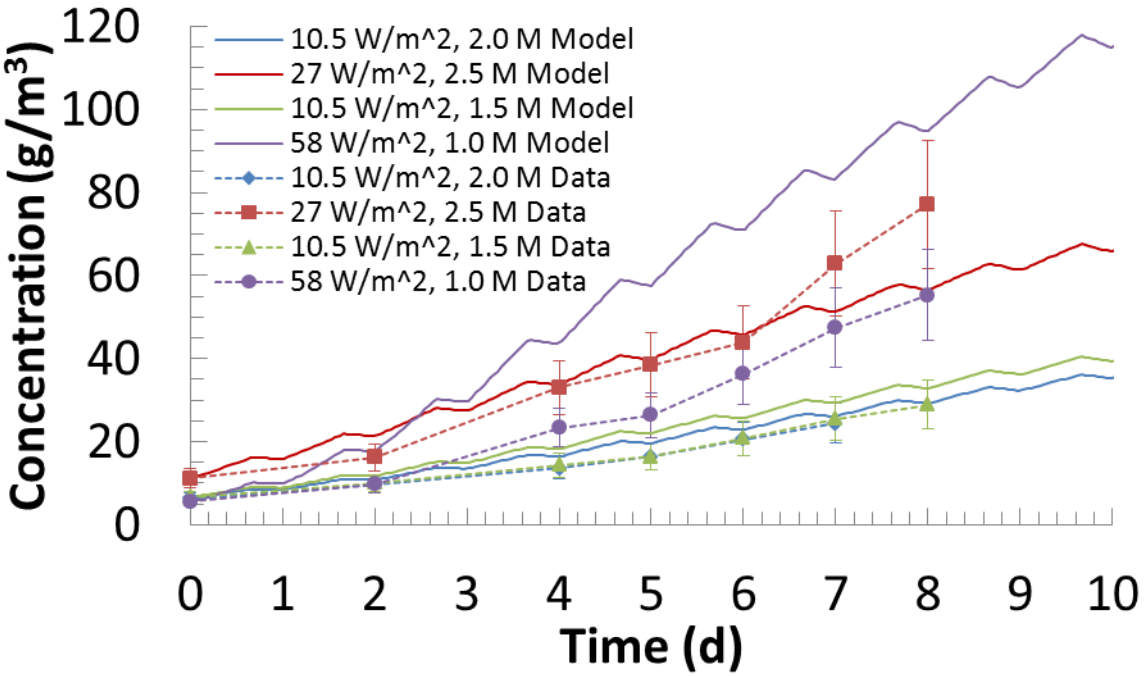

Figure 9. Plot of the predicted and measured *D. salina* concentration at laboratory scale over time at 31.5 °C and various light intensity and salinity conditions.

5.2.3. Nannochloropsis salina

The model includes the initial nutrient concentrations for the 2/F medium of 0.882 mM NO_3 (12.35 gN/m^3) and 0.0362 mM PO_4 (1.12 gP/m^3). The CO_2 is set initially to 0.9 g/m^3 [39]. The absorption of CO_2 into the media from the bubbling of air is assumed to be much more than sufficient to sustain this amount of CO_2 (2.31 µg/s). The initial algae concentrations are specified to match the initial measured concentrations.

Figure 10 – Figure 13 show the algae concentrations from measurements and simulation over time at temperatures of 18°C, 22°C, 26°C, and 30°C, respectively, and various light intensities and NaCl concentrations. For the most part, the data fit well to the calibrated model.

For the best fit between the model and measurements, the ideal growth conductions for *N. salina* are determined to be a NaCl concentration of 0.35 M, a light intensity of 20 W/m^2, and a temperature between 21.5 and 23.5°C. The maximum measured daily average growth rate in this study is 0.55 1/d, which when divided by 2/3 for the fraction of the day with light gives 0.825 1/d as the maximum instantaneous growth rate. The theoretical maximum productivity, P_M, used in equation (2) is determined to be 2.5 1/d. The typical trends were observed, the growth rate diminished at temperatures and salinities above and below the optimal value. The growth rate also diminished at light intensities below the optimal intensity and leveled out at higher intensities. Although pigment change was observed at the highest light intensity, we did not observe a decrease in growth rate.

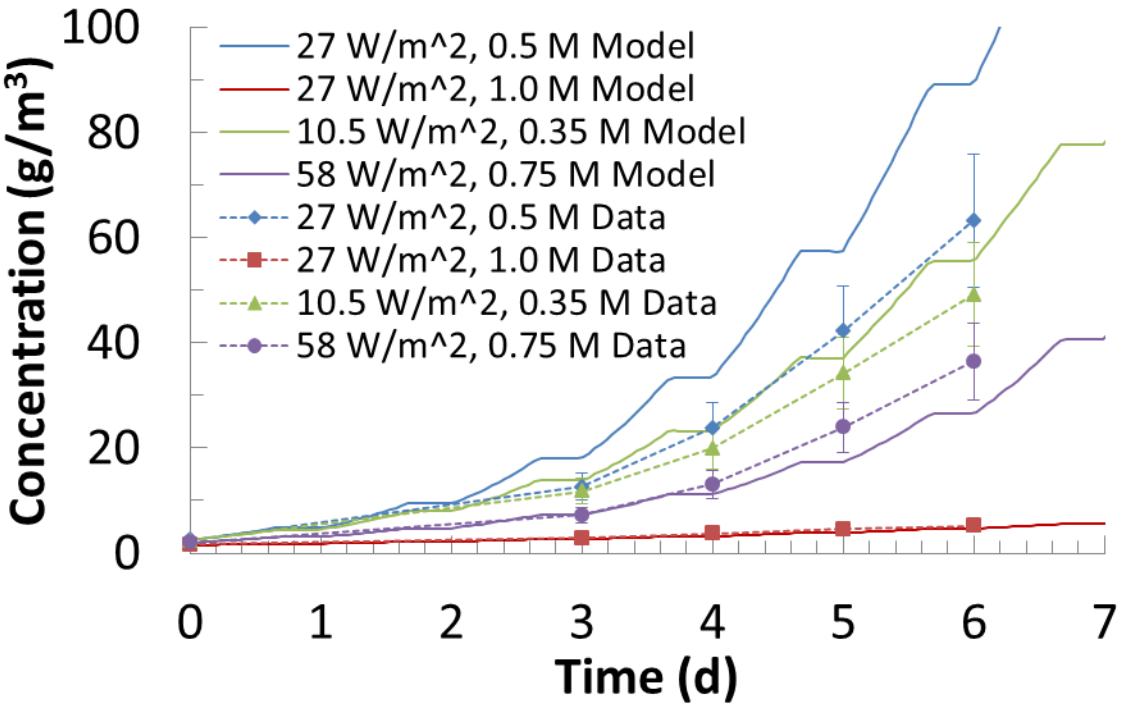

Figure 10. Plot of the predicted and measured *N. salina* concentration at laboratory scale over time at 18 °C and various light intensity and salinity conditions.

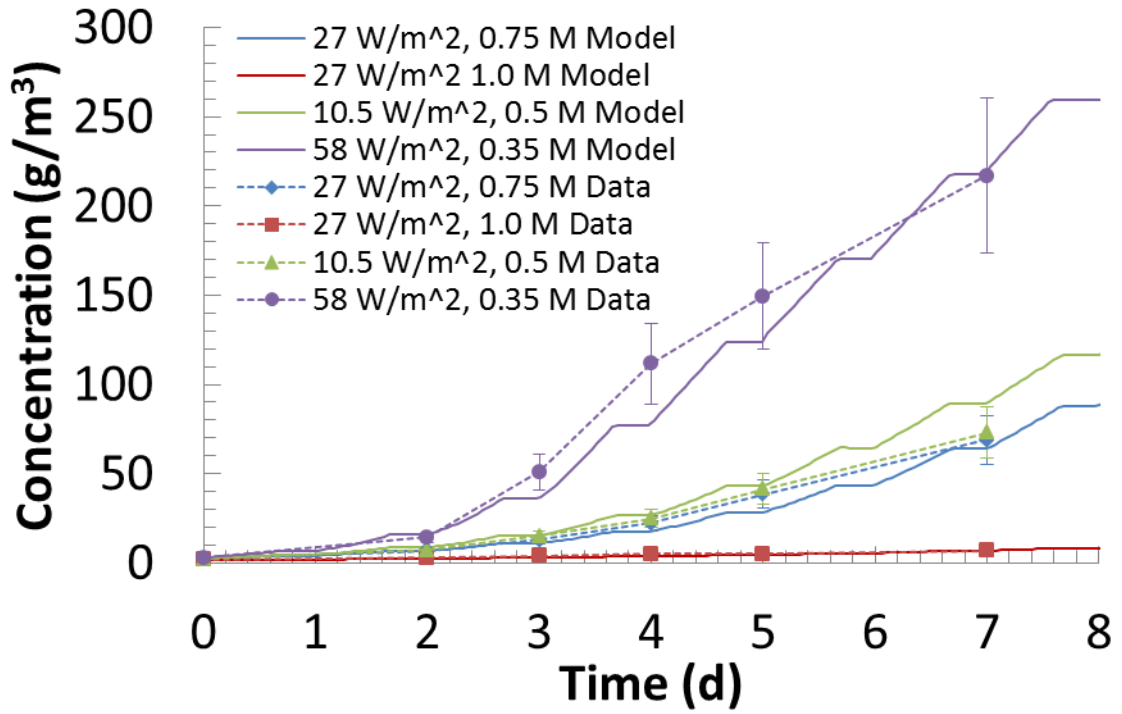

Figure 11. Plot of the predicted and measured *N. salina* concentration at laboratory scale over time at 22 °C and various light intensity and salinity conditions.

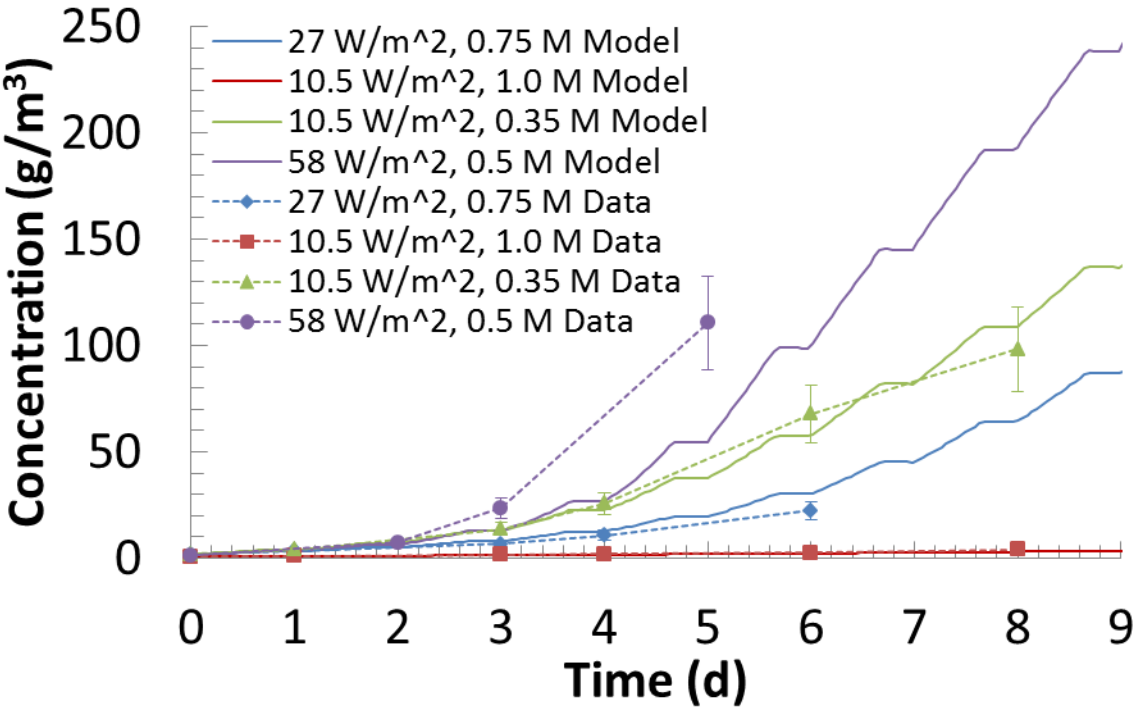

Figure 12. Plot of the predicted and measured *N. salina* concentration at laboratory scale over time at 26 °C and various light intensity and salinity conditions.

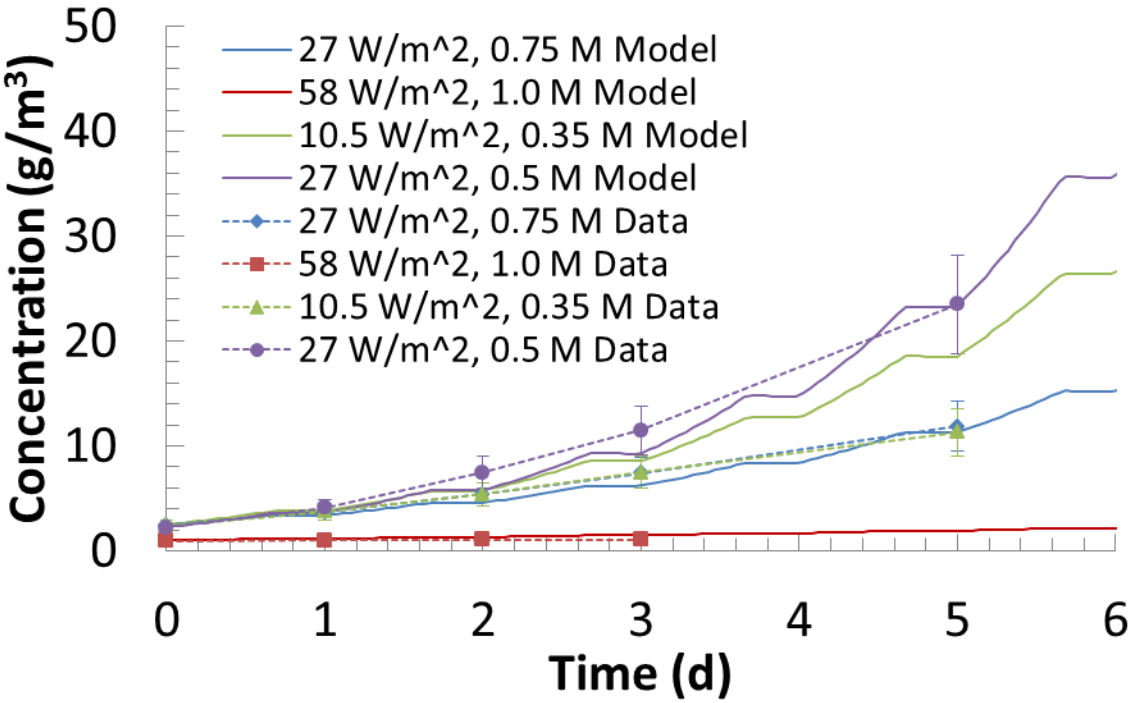

Figure 13. Plot of the predicted and measured *N. salina* concentration at laboratory scale over time at 30 °C and various light intensity and salinity conditions.

5.3. Greenhouse ponds

The model calibration from the *N. salina* laboratory measurements are applied to the greenhouse setup. The pond is simulated as a fully mixed 1.67 x 1.5 m^2 rectangular pond with a 0.211 m depth consisting of approximately 0.53 m^3 volume of medium. The light and temperature conditions experience by the ponds for the duration of the measurement are shown in Figure 14.

A laboratory grown culture of *N. salina* were inoculated into two ponds (west and east) at the greenhouse located at Sandia in Tech Area III. The ponds are circular with a radius of 0.9 m and a medium depth of 0.211 m. The experiment consisted of measuring the two ponds during a two-week period of time in November 2011.

The two ponds were operated at different CO_2 levels. The first week, the west pond was bubbled at 3 scfh CO_2, while the east pond only had ambient CO_2 levels. The second week the CO_2 levels were swapped for the two ponds. Following this two week experiment, the ponds were crashed with the use ~0.005% (v/v) sodium hypochlorite. Initial nitrate and phosphate concentrations were 54.7 and 3.1 g/m^3, respectively, equating to initial N and P concentrations of 12.36 and 1.01 g/m^3, respectively. During the measurement the west pond crashed, so we model the first 7 days of the west pond and the full 17 days for the east pond.

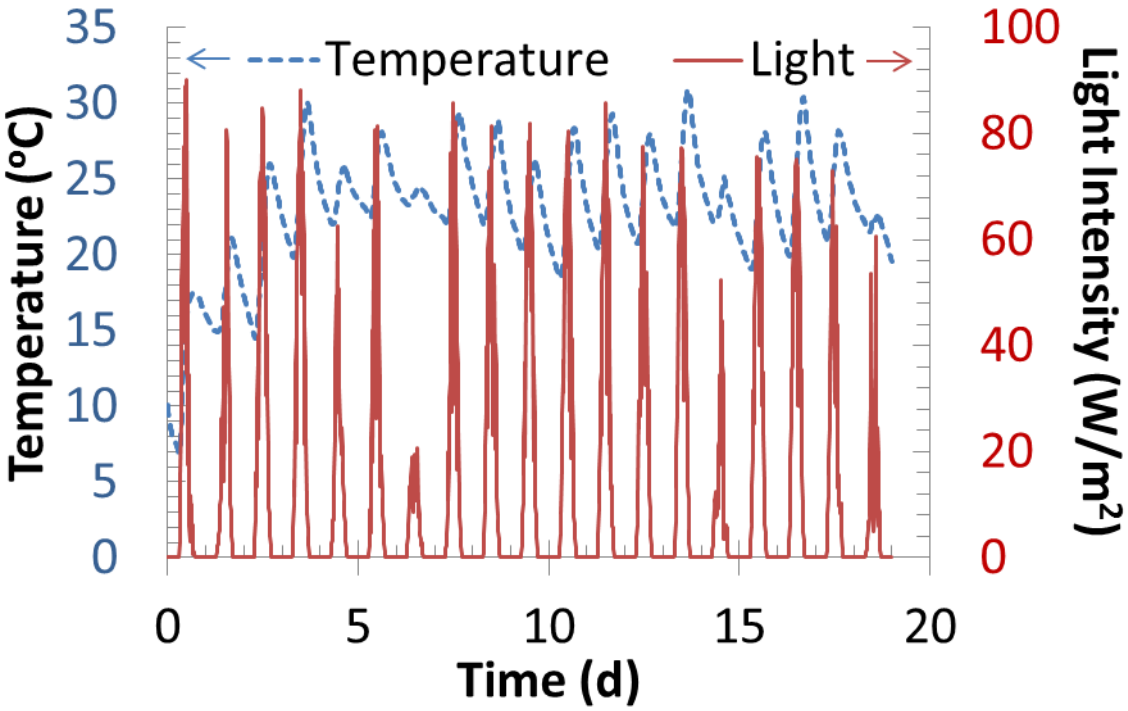

Figure 14. Plot of the light intensity and temperature over time for the greenhouse pond measurement.

The results from the measurements and the model are plotted in Figure 15. The model does well to predict the difference between the two ponds operating with different CO_2 sources during the first 7 days when the ponds are healthiest. However, later in the pond runs the model begins to

over predict the growth. This may be due to contamination over time as the pond is exposed to other biological species.

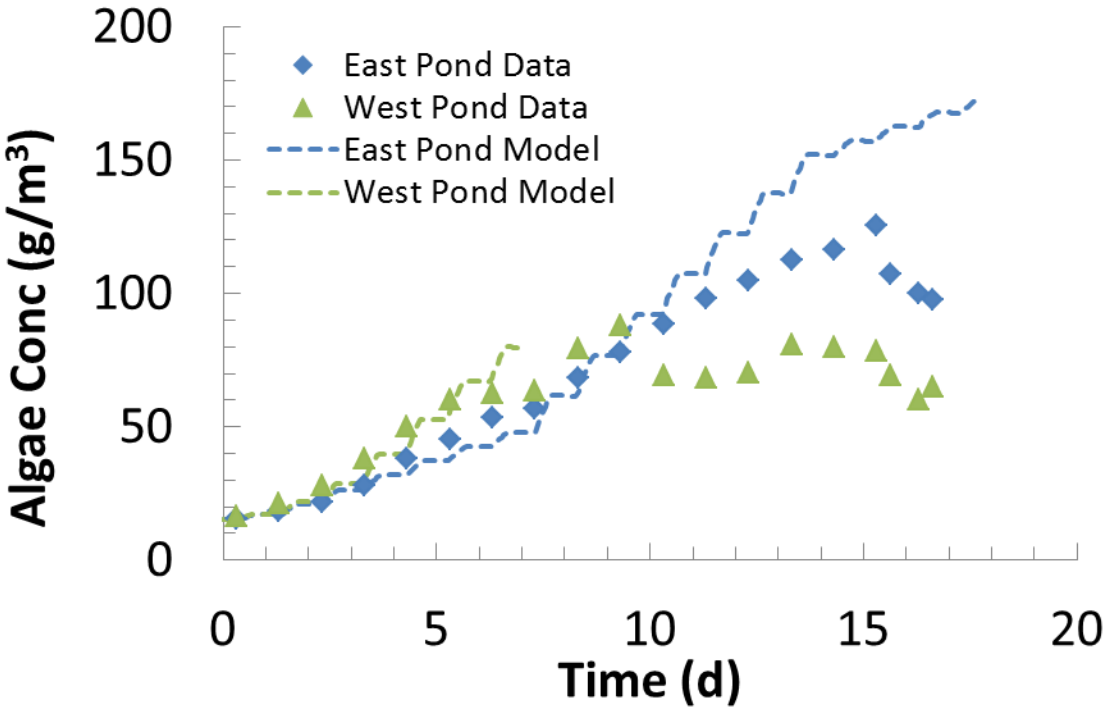

Figure 15. Plot of the measured and predicted algae concentration over time for the greenhouse ponds.

The three main contributors to limiting the algal growth in the greenhouse pond are the light, temperature, and CO_2 concentration. The limitation factors for each of these are plotted in Figure 16. For this case, the ideal light and temperature are well aligned. However, the CO_2 concentration drops to limiting levels during the high growth periods with ideal light and temperature, which causes the growth to be limited at all times even in the high CO_2 concentration bubbling case.

The instantaneous growth rate from the model and the daily average growth rate from the measurements are plotted in Figure 17. The maximum instantaneous growth rate achieved was 1.2 1/d and corresponds to a brief period where all the limitation factors are close to 1. Due to the high temperatures experienced in Albuquerque, NM during the summer, the greenhouse measurement was conducted during the winter months. This limited the fraction of the day with usable light to less than 0.5. Thus, if the CO_2 could be kept high enough to not be limiting and the days could be longer while keeping the temperature reasonable, the growth in the greenhouse ponds could have been at the 1.2 1/d level for longer periods of time and yielded higher productivity.

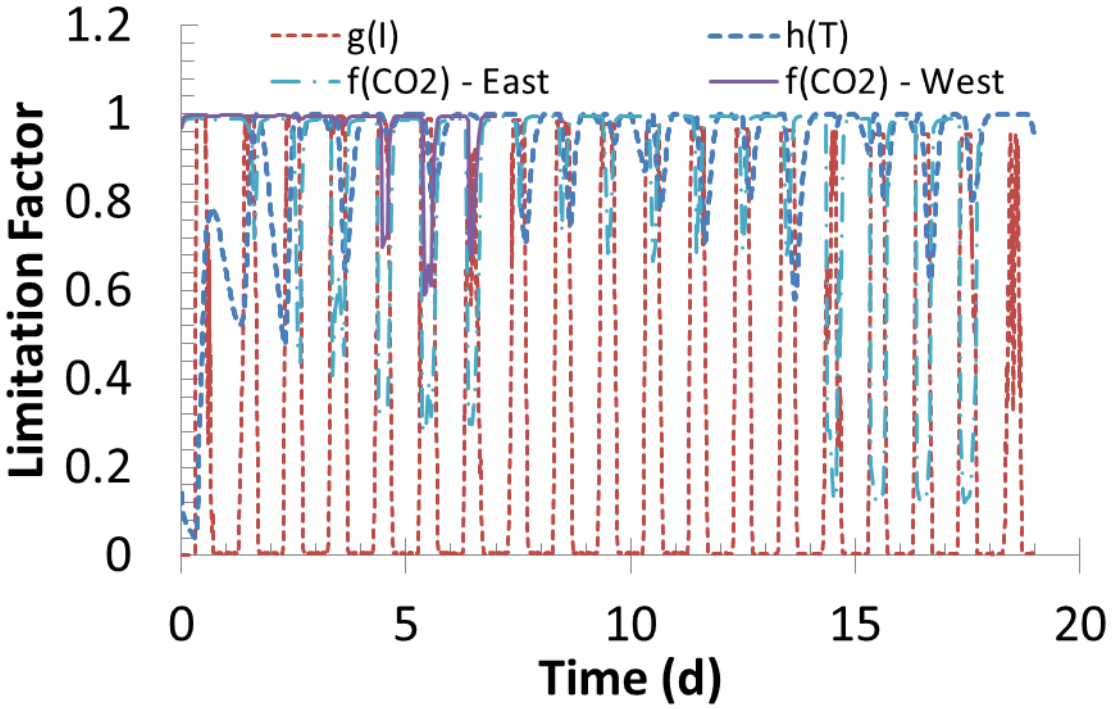

Figure 16. Plot of the limitation factors over time for the greenhouse pond measurement.

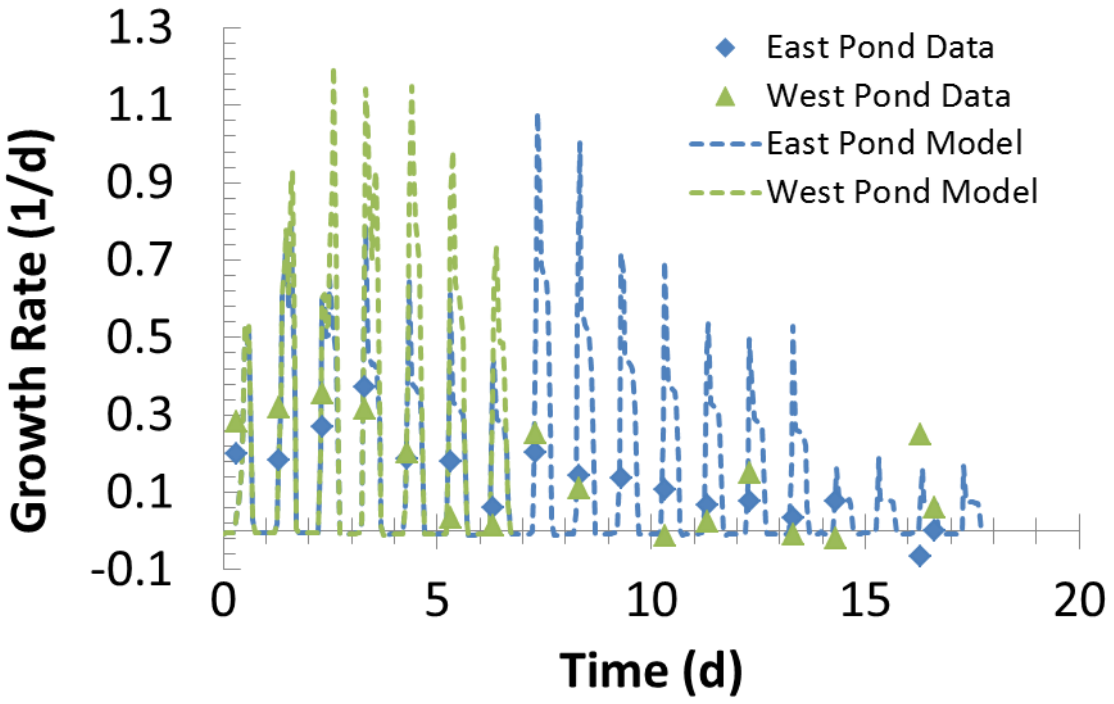

Figure 17. Plot of the measured daily average and predicted instantaneous growth rates over time for the greenhouse ponds.

5.4. Open-channel Raceway

The model calibration from the laboratory setup is applied to the open-channel raceway conditions. The raceway is simulated as a fully mixed 126 x 2.44 m^2 rectangular pond with a 0.15 m depth consisting of approximately 46 m^3 volume of medium. The light and temperature conditions experience by the raceway for the duration of the measurement are shown in Figure 18. The initial nutrient conditions are assumed to be the same as the greenhouse case. The CO_2 for this case is assumed to be bubbled in and incorporated via the paddle wheel fast enough to not limit the growth.

The results for algae concentration over time from the measurements and the model are plotted in Figure 19. As with the greenhouse pond, the model does well to predict the algal concentration over time in the raceway.

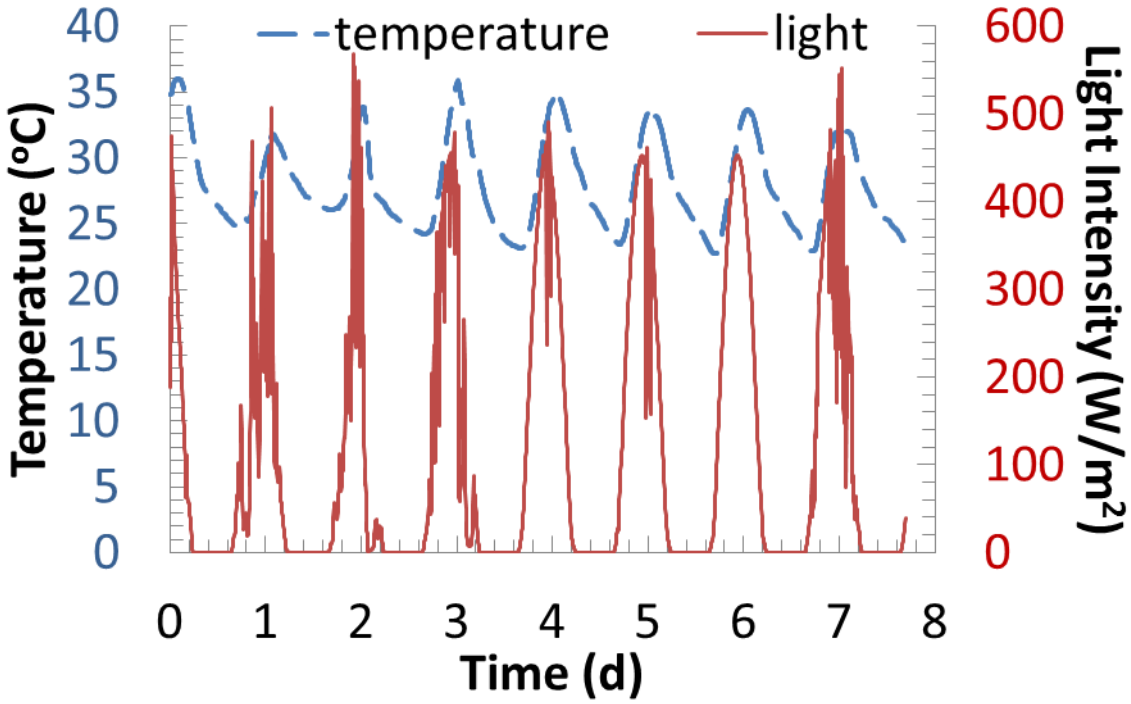

Figure 18. Plot of the light and temperature conditions over time for the open-channel raceway.

The two contributors to limiting the algal growth for this case are the light and temperature. The limitation factors for each of these are plotted in Figure 20. For this case, the ideal light and temperature are not in phase. When the light is high the temperature of the pond becomes too hot and growth is limited and when the light is limiting the temperature reduces to more optimal values. This causes most of the growth to occur in the morning and evening periods, while at mid-day and at night the growth is highly limited. This is demonstrated by the product of the light and temperature limitation factors plotted in Figure 20. The product dips mid-day and peaks in the morning and afternoon. From this information, one could imagine algae with a higher temperature tolerance that could perform better in these conditions.

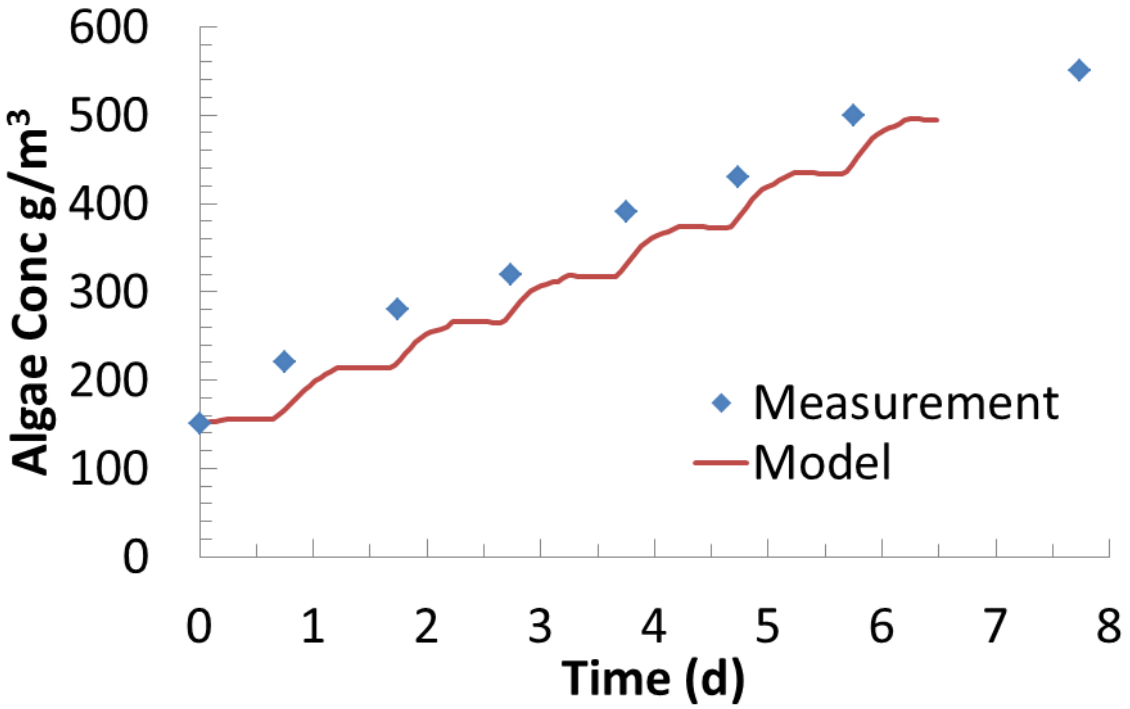

Figure 19. Plot of the measured and predicted algae concentration over time the open-channel raceway.

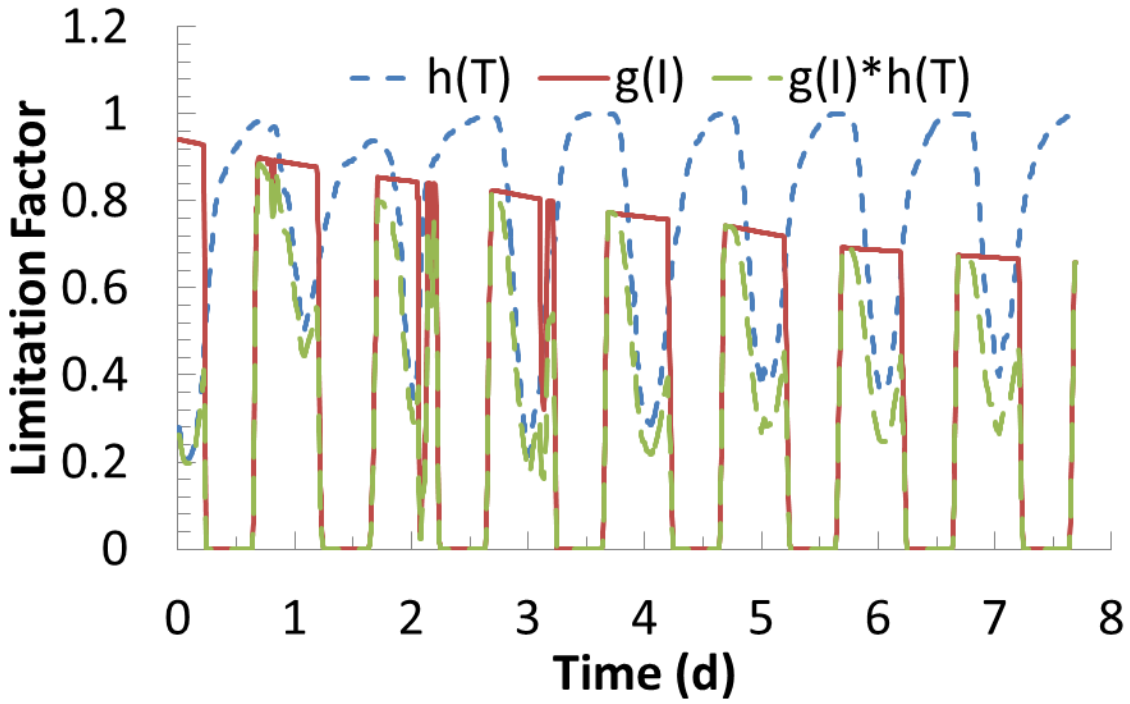

Figure 20. Plot of the limitation factors over time for the open-channel raceway.

The instantaneous growth rate from the model and the daily average growth rate from the measurements are plotted in Figure 21. The maximum instantaneous growth rate achieved was

0.9 1/d. The concentration of the algae is much higher in the raceway case than in either the lab or the greenhouse pond cases. This results in a greater reduction in the light penetration and thus the growth. Additionally, since the period of the highest light is growth limited by temperature, the peak achievable performance is never realized.

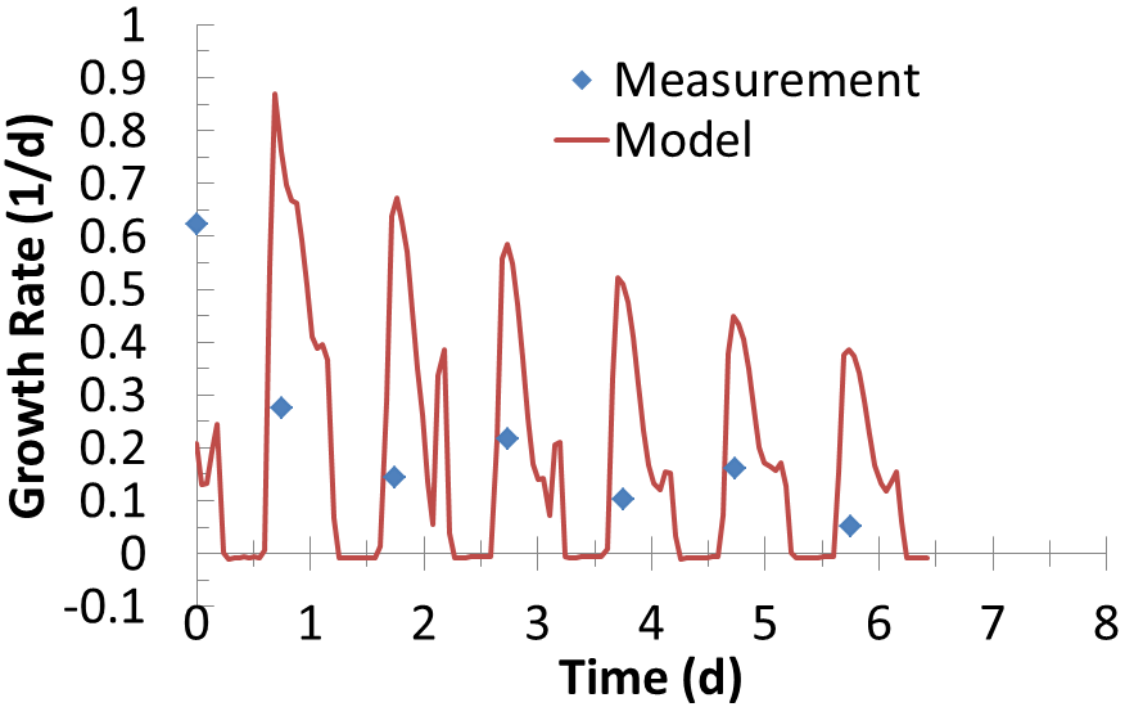

Figure 21. Plot of the measured daily average and predicted instantaneous growth rates over time for the open-channel raceway.

5.5. Conclusion

The model has been validated by comparing the prediction between the calibrated model for *N. salina* and measurement results for two large scale cultivation systems: greenhouse ponds and an open-channel raceway. The results show that the model can help identify which factors are causing the growth to be limited, which will help optimize bioreactor designs and improve algae strain selection.

6. FLUENT IMPLEMENTATION

6.1. Introduction

The current version of the EFDC fluid dynamics model is cumbersome and limited to open-channels. A more user friendly and versatile CFD code is needed to enable the simulation of a wider variety of bioreactors including close photobioreactors. A commercial fluid dynamics code, such as FLUENT, provides a verified, validated, and versatile CFD code. The use of user defined functions (UDF) would allow for the modification of existing code to include phenomena not directly included within the commercial code.

6.2. CFD Model

A representative geometry of the cross section of a typical algae raceway can be used to simulate the pond as a whole (see Figure 22). At a minimum, only the straight portion needs to be modeled because at commercial scale the bends will amount to only a small portion of the raceway and will, most likely, not significantly affect the overall growth of algae. The number of computation cells was set in order to ensure resolution of light as a function of depth and to ensure that the ratio of length to width of each cell remained small enough to create a stable domain. In addition, the time step was chosen to maintain stability during transient simulations. ANSYS Fluent, version 13.1 was used for all simulations.

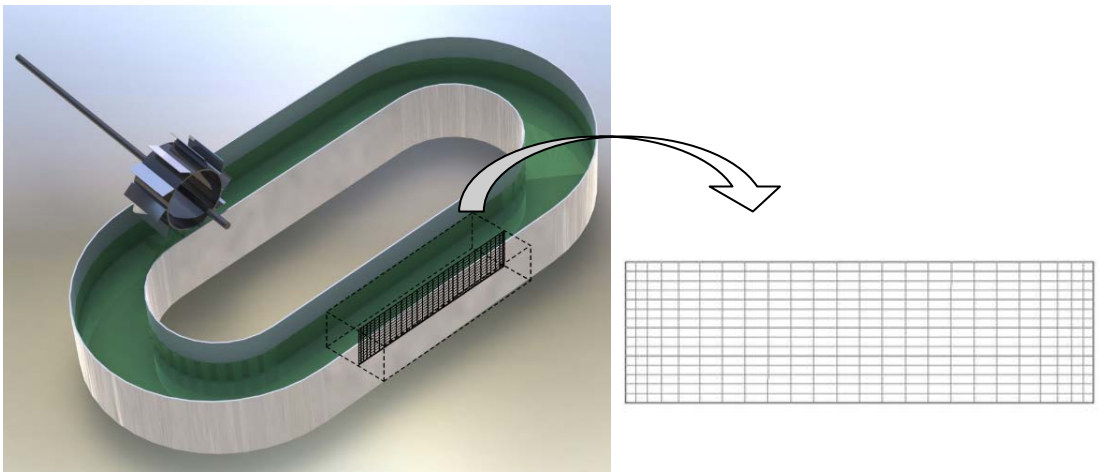

Figure 22. Two-dimensional computational domain of the CFD model, 0.3 m deep by 1 m long.

6.3. User Defined Functions

The use of user defined functions (UDF) allows for the modeling of transport phenomena and material properties not directly coded into CFD software such as, algal growth and nutrient depletion. In addition, the UDF can be used to define boundary and initial conditions, weather conditions as a function of time, and properties such as density. The UDF has been written, in the C programing language, to calculate the algal and nutrient fluxes, which are then passed to the CFD software to be included in the source term when solving the mass conservation equation. A flow chart of the interaction between the CFD software and the UDF can be seen in Figure 23.

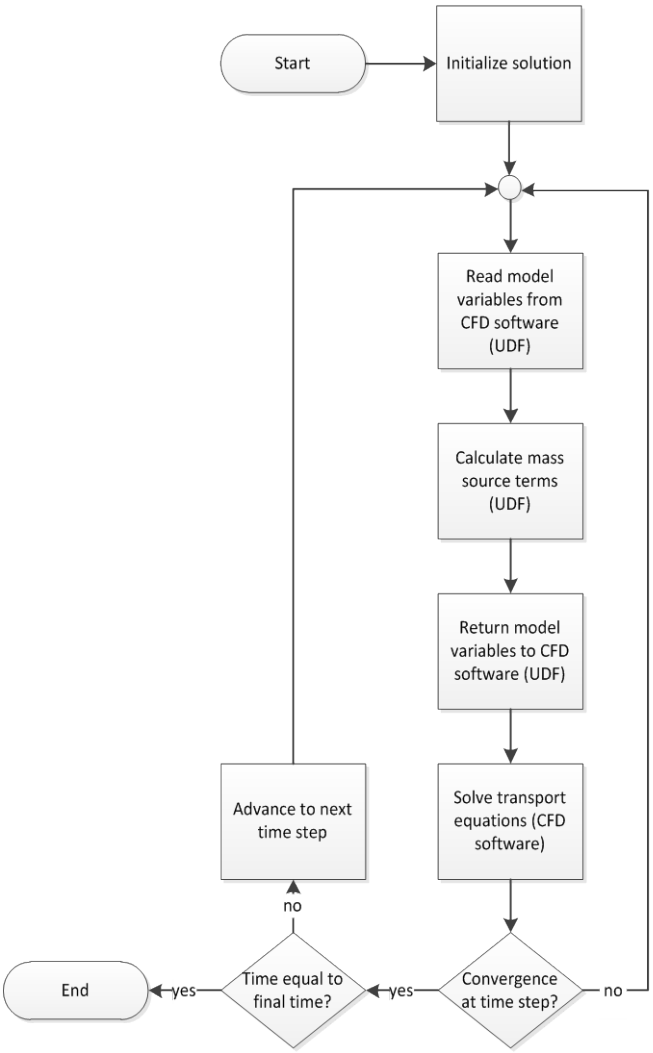

Figure 23. Flow chart the interaction between the computational fluid dynamics (CFD) software and the user defined functions (UDF).

6.4. Fluent Model Verification

The model can output a number of spatiotemporal parameters including species concentrations, temperature profiles, any of the variables calculated by the UDF, and many others. In order to ensure that the model functions correctly and contains no coding errors, an example problem with a known solution was solved and used to validate the model. The model was then used to simulate algal growth in a greenhouse pond and compared to experimental data and an existing water quality and hydrodynamic model, EFDC. In addition to the CFD model a simplified model was constructed using a fourth order Runge Kutta method, in Matlab, in order to ensure the CFD code was functioning properly and free of bugs. The model is a single computational cell.

6.4.1. Example with known numerical solution

The numerical solution of example 33.2 from Chapra [40], using a fourth order Runge-Kutta method, was compared with the numerical results obtained from the CFD code modified through UDF. The system is assumed to be a fully mixed, batch system; therefore, the concentration of chlorophyll-a, a function of algae concentration, and phosphorous can be found through a mass balance of the system. For the CFD model, algae and phosphorous are considered to be at low enough concentrations such that they do not affect the properties of the water within the computational domain. The boundary and initial conditions can be seen in Table 1 and results of the simulations can be seen in Figure 24. The CFD model was found to be in good agreement with the fourth order Runge Kutta solution of the Chapra problem, indicating that the UDF is functioning correctly.

Table 1. Initial and boundary for the Chapra problem.

Parameter	Unit	Values[a]
C_p[b]		1.5
I_o	ly day^{-1}	400
I_s	ly day^{-1}	250
K_B	m^{-1}	0.1
B_M	1/s	1.57E-07
K_P^h	kg m^{-3}	2.00E-06
photo period		0.5
P_m	s^{-1}	1.57E-05
z	m	10
B_0	kg m^{-3}	5.00E-07
P_0	kg m^{-3}	9.70E-06

[a] [40]

[b] C_p= ratio of P to chlorophyll-a

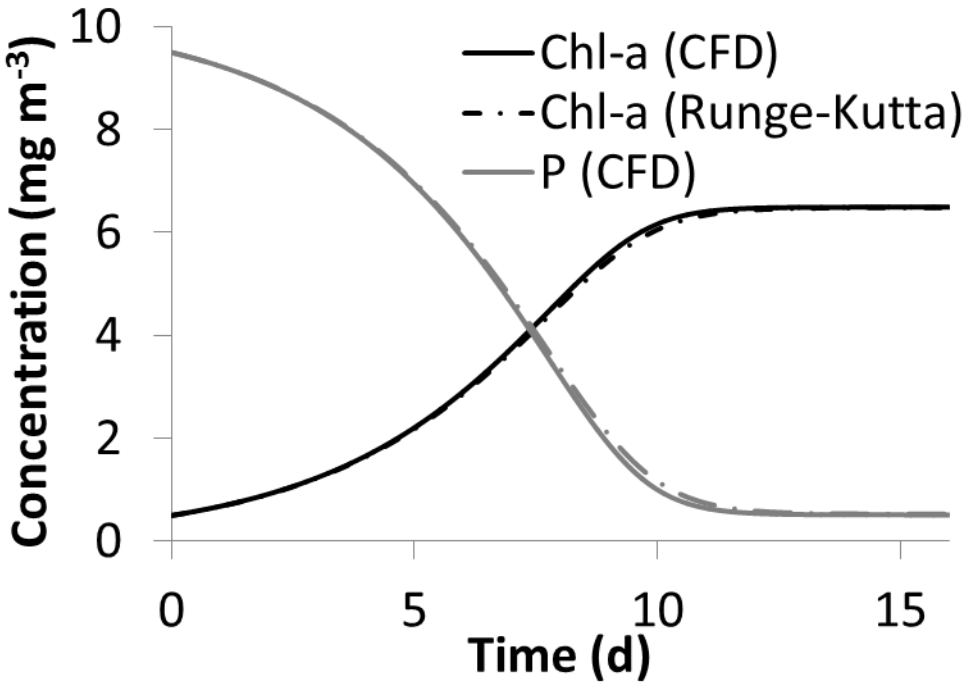

Figure 24. Chlorophyll-a and phosphorous concentration as a function of time for the Chapra problem.

6.4.2. Greenhouse Model

The model was then used to simulate data from a greenhouse experiment and was compared to an EFDC model for the same experiment. *Nannochloropsis salina* was grown in a 0.9 m radius by 0.211 m deep pond within a greenhouse under known conditions of temperature, irradiance, and pH. Algal growth was modeled as a function of nutrients, temperature, light intensity, and pH for a period of 14 days. Carbon dioxide concentrations were used to calculate the nutrient limitation function but were decoupled from pH since that data was available experimentally.

6.4.2.1. Without Carbon Dioxide Exchange

The preliminary model did not include exchange of carbon dioxide with the atmosphere. This way a carbon balance of the system could be easily carried out to ensure conservation of mass within the computational domain. The initial and boundary conditions, as well as model constants can be seen in Table 2. The computational domain was assumed to be fully mixed. Algal growth as a function of time for the EFDC, Runge-Kutta, and CFD models can be seen in Figure 25, while carbon dioxide concentration as a function of time can be seen in Figure 26. The values of carbon dioxide vary slightly between the EFDC and CFD models due to the linear averaging employed by EFDC.

Table 2. Greenhouse model parameters without exchange of carbon dioxide.

Parameter	Unit	Values [41]
B:C [a]		45:1
C:N:P [b]		358:38:01
CO_2 flow rate	kg m^{-3} s^{-1}	4.4e-7 or 1.7e-6
$I_{s,min}$	W m^{-2}	17
K_1^T	$°C^{-2}$	0.69
K_2^T	$°C^{-2}$	0.007
K_B	m^{-1}	0.45
B_M	s^{-1}	1.57E-07
K_c^h	kg m^{-3}	2.80E-05
k_c	m m^3 (g B)$^{-1}$	0.314
K_n^h	kg m^{-3}	1.00E-05
$K_{OM,n}$	s^{-1}	1.7E-07
$K_{OM,p}$	s^{-1}	1.2E-06
K_p^h	kg m^{-3}	2.00E-06
P_m	s^{-1}	1.2E-05
T_1	°C	18
T_2	°C	22
B_0	kg m^{-3}	1.54E-02
C_0	kg m^{-3}	9.00E-04
N_0	kg m^{-3}	5.47E-02
P_0	kg m^{-3}	3.10E-03

[a] ratio of algal biomass to carbon, [b] ratio of carbon to nitrogen to phosphorous in algal biomass

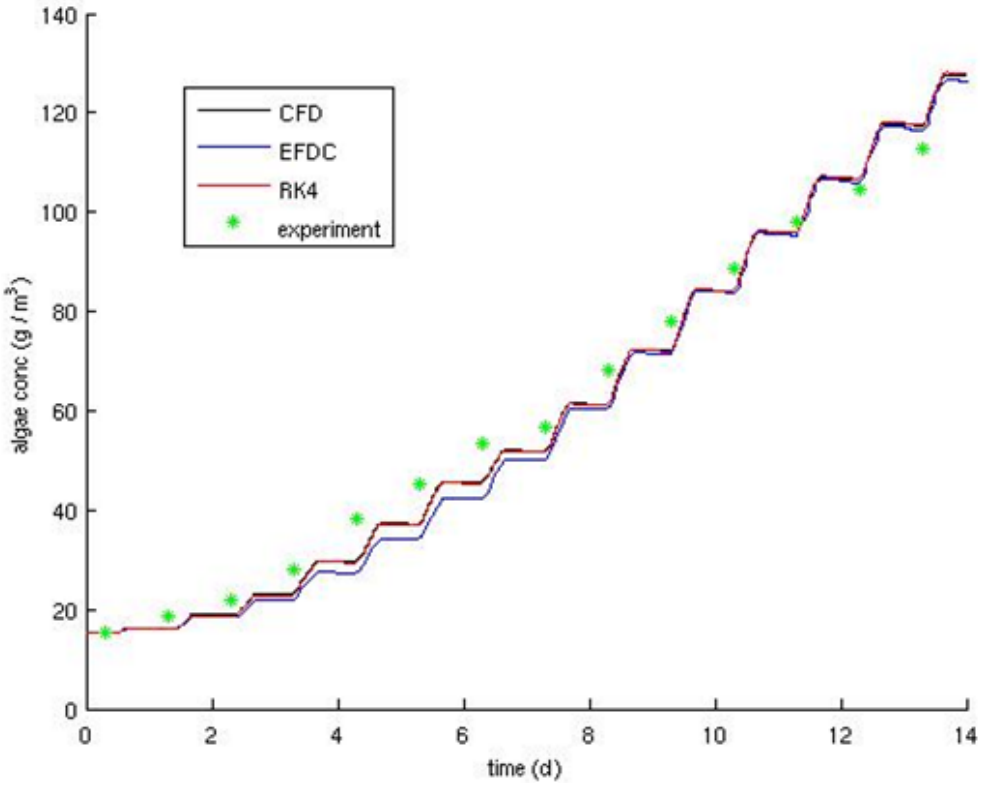

Figure 25. Algae concentration as a function of time for the CFD, EFDC, and Runge Kutta models along with experimental data from a greenhouse experiment.

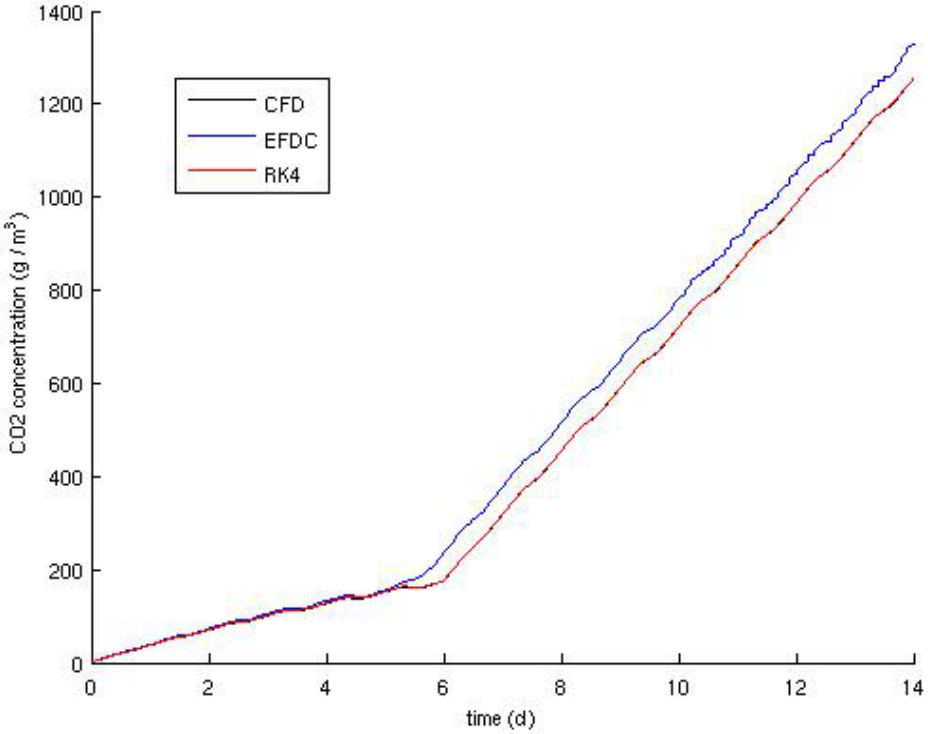

Figure 26. Carbon dioxide concentration as a function of time for the CFD, EFDC and Runge Kutta models without gas exchange with the surface.

6.4.2.2. With Carbon Dioxide Exchange

Exchange of carbon dioxide with the atmosphere was added to the CFD model. Henry's law was used to define the saturation concentration of carbon dioxide within the pond and the rate of carbon dioxide exchange was defined as $6.2\ 10^{-5}$, with all other parameters the same as with no carbon dioxide exchange. The values of algae and carbon dioxide for the three models can be seen in Figure 27 and Figure 28, respectively. The values of carbon dioxide between the CFD and EFDC models are not identical due to different aeration functions; however, the overall trend is the same.

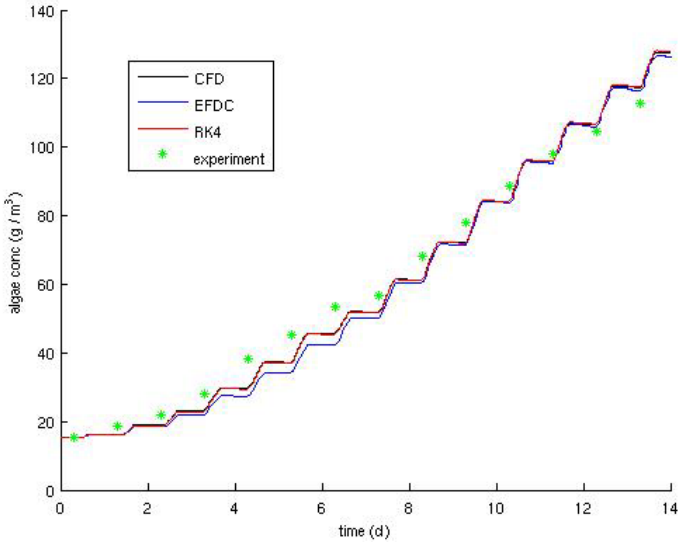

Figure 27. Algae concentration as a function of time for the CFD, EFDC, and Runge Kutta models along with experimental data from a greenhouse experiment, assuming carbon dioxide transfer with the surface.

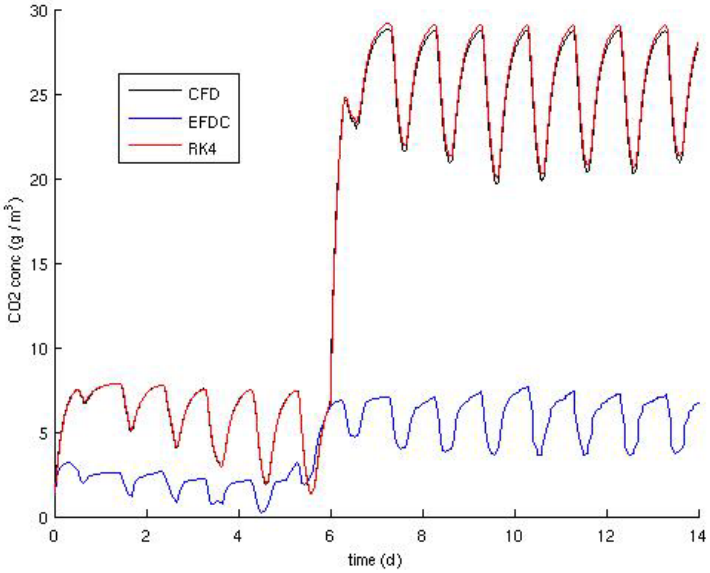

Figure 28. Carbon dioxide concentration as a function of time for the CFD, EFDC and Runge Kutta models without gas exchange with the surface.

In Figure 29, it can be seen that the actual concentration tracks the saturation concentration of carbon dioxide within the pond when algal growth is turned off.

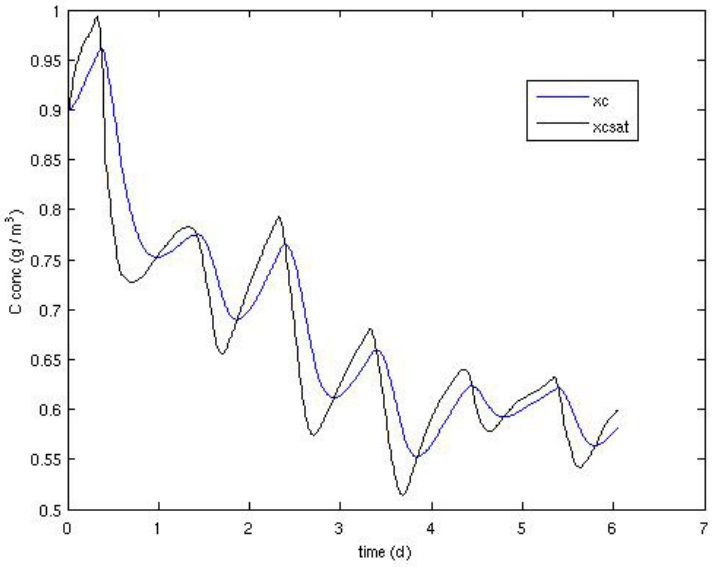

Figure 29. Graph of the actual (xc) and saturation (xcsat) concentrations of carbon dioxide when algal growth is not present.

6.5. Conclusion

Once thoroughly validated, this model shows promise to serve as a tool for predicting algal biomass production based on pond design and operation, algae species, and weather conditions. The ease with which this model can be adapted to suit any scenario will allow for its application to commercial or research projects. The validation conducted demonstrates that the UDF is accurately calculating biomass production in comparison with existing examples and codes. Expansion of the model to include terms for lipid accumulation, particle tracking, wind forcing, and more advanced radiation models will only serve to make the model more accurate. The current results obtained using this model show that CFD, when combined with UDF, can accurately predict biomass and thereby serve as a cost and time effective method for designing and optimizing open ponds for biomass production.

7. CONCLUSIONS

Multifactorial measurements of *N. salina* and *D. salina* have been conducting to populate the empiricisms of the CE-QUAL model of algae growth kinetics. The effect of salinity on green-algae growth has been added to the model to simulate marine algal species. The CE-QUAL model was implemented into FLUENT to expand the CFD capabilities. The laboratory calibrated model for *N. salina* has been validated with two large scale studies. The model predicts the growth trends in greenhouse ponds and an open-channel raceway well. The calibrated model was used to analyze which environmental factors are causing the growth to be limited. This model could be used to study scale-up effect through comparisons of the lab scale kinetics and a larger scale system looking at the effects of predation, depth-decay of light (light extinction) in the culture, and optimized CO_2 delivery. The model can then be expanded to study growth in production scale photobioreactors and open-channel raceways eliminating the need for expensive large-scale experiments. As more multifactorial data are accumulated for a variety of algal strains, the model can be used to select appropriate algal species for various geographic and climatic locations.

8. REFERENCES

1. US-DOE, *National Algal Biofuels Technology Roadmap*, 2009, Office of Energy Efficiency and Renewable Energy and Office of Biomass: Albuquerque, NM.
2. Goss, R. and C. Wilhelm, *Lipids in algae, lichens, and mosses*, in *Lipids in Photosynthesis: Essential and Regulatory Functions*, H. Wada and E. Murata, Editors. 2009, Springer Science & Business Media. p. 117.
3. Hu, Q., et al., *Microalgal triacylglycerols as feedstocks for biofuel production: perspectives and advances.* The Plant Journal, 2008. **54**: p. 621-639.
4. Kirst, G.O., *Salinity Tolerance of Eukaryotic Marine Algae.* Annual Review of Plant Physiology and Plant Molecular Biology, 1989. **40**: p. 21-53.
5. Brock, T.D., *Salinity and the Ecology of Dunaliella from Great Salt Lake.* Journal of General Microbiology, 1975. **89**: p. 285-292.
6. Auken, O.W.V. and I.B. McNulty, *The Effect of Environmental Factors on the Growth of a Halophylic Species of Algae.* Biological Bulletin, 1973. **145**: p. 210-222.
7. García, F., Y. Freile-Pelegrín, and D. Robledo, *Physiological characterization of Dunaliella sp. (Chlorophyta, Volvocales) from Yucatan, Mexico.* Bioresource Technology, 2007. **98**: p. 1359-1365.
8. Fabregas, J., et al., *Growth of the Marine Microalga Tetraselmis suecica in Batch Cultures with Different Salinities and Nutrient Concentrations.* Aquaculture, 1984. **42**: p. 207-215.
9. John C. Batterton, J. and C.V. Baalen, *Growth Response of Blue-green Algae to Sodium Chloride Concentration.* Archives of Microbiology, 1971. **76**: p. 151-165.
10. Pal, D., et al., *The effect of light, salinity, and nitrogen availability on lipid production by Nannochloropsis sp.* Applied Microbial and Cell Physiology, 2011. **90**: p. 1429-1441.
11. Sonnekus, M.J., *Effects of Salinity on the Growth and Lipid Production of Ten Species of Microalgae from the Swartkops Saltworks: A Biodiesel Perspective*, in *Faculty of Science*2010, Nelson Mandela Metropolitan University. p. 98.
12. Katz, A., et al., *In Vivo pH Regulation by a Na^+/H^+ Antiporter in the Halotolerant Alga Dunaliella salina.* Plant Physiology, 1991. **96**: p. 110-115.
13. Benemann, J.R., D.M. Tillett, and J.C. Weissman, *Microalgae biotechnology.* Trends in Biotechnology, 1987. **5**: p. 47-53.
14. Gómez, P.I. and M.A. González, *The effect of temperature and irradiance on the growth and carotenogenic capacity of seven strains of Dunaliella salina (Chlorophyta) cultivated under laboratory conditions.* Biological Research, 2005. **38**: p. 151-162.
15. Weldy, C.S. and M. Huesemann, *Lipid Production by Dunaliella salina in Batch Culture: Effects of Nitrogen Limitation and Light Intensity.* Journal of Undergraduate Research, 2007. **7**: p. 115-122.
16. Sarmad, J., M. Shariati, and A.H. Tafreshi, *Preliminary Assessment of β-carotene Accumulation in Four Strains of Dunaliella salina Cultivated under the Different Salinities and Low Light Intensity.* Pakistan Journal of Biological Sciences, 2006. **9**(8): p. 1492-1496.
17. Mendoza, H., et al., *Characterization of Dunaliella salina strains by flow cytometry: a new approach to select carotenoid hyperproducing strains.* Electronic Journal of Biotechnology, 2008. **11**(4).

18. Masuda, T., J.E.W. Polle, and A. Melis, *Biosynthesis and Distribution of Chlorophyll among the Photosystems during Recovery of the Green Alga Dunaliella salina from Irradiance Stress.* Plant Physiology, 2002. **128**: p. 603-614.
19. Markovits, A., et al., *Strain selection for β-carotene production by Dunaliella.* World Journal of Microbiology and Biotechnology, 1993. **9**: p. 534-537.
20. Marín, N., et al., *Effect of nitrate concentration on growth and pigment synthesis of Dunaliella salina cultivated under low illumination and preadapted to different salinities.* Journal of Applied Phycology, 1998. **10**: p. 405-411.
21. Haghjou, M.M. and M. Shariati, *Photosynthesis and Respiration under Low Temperature Stress in Two Dunaliella Strains.* World Applied Sciences Journal, 2007. **2**(4): p. 276-282.
22. Giordano, M. and G. Bowes, *Gas Exchange and C Allocation in Dunaliella salina Cells in Response to the N Source and CO_2 Concentration Used for Growth.* Plant Physiology, 1997. **115**: p. 1049-1056.
23. García-González, M., et al., *Conditions for open-air outdoor culture of Dunaliella salina in southern Spain.* Journal of Applied Phycology, 2003. **15**: p. 177-184.
24. Borowitzka, L.J., M.A. Borowitzka, and T.P. Moulton, *The mass culture of Dunaliella salina for fine chemicals: From laboratory to pilot plant.* Hydrobiologia, 1984. **116**: p. 115-134.
25. Neidhardt, J., et al., *Photosystem-II repair and chloroplast recovery from irradiance stress: relationship between chronic photoinhibition, light harvesting chlorophyll antenna size and photosynthetic productivity in Dunaliella salina (green algae).* Photosynthesis Research, 1998. **56**: p. 175-184.
26. Al-Hassan, R.H., et al., *Correlative Changes of Growth, Pigmentation and Lipid Composition of Dunaliella salina in Response to Halostress.* Journal of General Microbiology, 1987. **133**: p. 2607-2616.
27. Abu-Rezq, T.S., S. Al-Hooti, and D.A. Jacob, *Optimum culture conditions required for the locally isolated Dunaliella salina.* Journal of Algal Biomass Utilization, 2010. **1**(2): p. 12-19.
28. Boussiba, S., et al., *Lipid and Biomass Production by the Halotolerant Microalga Nannochloropsis salina.* Biomass, 1987. **12**: p. 37-47.
29. Cerco, C.F. and T. Cole, *User's Guide to the CE-QUAL-ICM Three-Dimensional Eutrophication Model, Release Version 1.0,* 1995, U.S. Army Corps of Engineers.
30. James, S.C. and V. Boriah, *Modeling Algae Growth in an Open-Channel Raceway.* Journal of Computational Biology, 2010. **17**(7): p. 895-906.
31. James, S.C. and V. Janardhanam. *An Algae-Growth CFD Model Including the Effects of CO_2 Concentration and pH*. in *Algae Biomass Summit*. 2011. Minneapolis, MN.
32. Monod, J., *The growth of bacterial cultures.* Annual Review of Microbiology, 1949. **3**: p. 371-394.
33. DiToro, D., S. O'Connor, and R. Thormann, *A dynamic model of the phytoplankton population in the Sacramento-San Joaquin Delta,* in *Nonequilibrium systems in water chemistry*1971, American Chemical Society. p. 131-180.
34. DiToro, D.M., Donald J. O'Connor, *Phytoplankton-Zooplankton-Nutrient Interaction Model for Western Lake Erie.* Ecology, 1975. **3**: p. 423 - 473.
35. Cossins, A.R. and K. Bowler, *Temperature Biology of Animals*1987, New York, NY: Chapman and Hall. 339.

36. Cerco, C.F. and T. Cole, *Three-dimensional eutrophication model of Chesapeake Bay*, 1994, US Army Corps of Engineers. p. 658.
37. Redfield, A.C., *On the proportions of organic derivatives in sea water and their relation to the composition of plankton*, in *James Johnstone Memorial Volume*, R.J. Daniel, Editor 1934, University Press of Liverpool: London. p. 176-192.
38. Hecky, R.E., P. Campbell, and L.L. Hendzel, *The stoichiometry of carbon, nitrogen, and phosphorus in particulate matter of lakes and oceans.* Limnology and Oceanography, 1993. **38**(4): p. 709-724.
39. Burkhardt, S., I. Zondervan, and U. Riebesell, *Effect of CO_2 concentration on C:N:P ratio in marine phytoplankton: A species comparison.* American Society of Limnology and Oceanography, 1999. **44**(3): p. 683-690.
40. Chapra, S.C., *Surface water-quality modeling*. McGraw-Hill Series in Water Resources and Environmental Engineering1997, New York: McGraw-Hill.
41. James, S.C., V. Janardhanam, and D.T. Hanson, *Simulating pH Effects in an Algae-Growth Hydrodynamics Model.* Journal of Phycology, 2013. **Submitted**.

DISTRIBUTION (ALL ELECTRONIC COPY)

1	MS0895	Jerilyn A. Timlin	08622
1	MS0895	Howland D.T. Jones	08622
1	MS1413	Aaron. M. Collins	08622
1	MS1413	Anne Ruffing	08622
1	MS1413	Kylea Parchert	08622
1	MS1413	Christine Trahan	08622
1	MS1413	James Carney	08622
1	MS1413	Amy J. Powell	08635
1	MS9054	Art E. Pontau	08360
1	MS9056	Thomas A. Reichardt	08128
1	MS9159	Jerry McNeish	08954
1	MS9291	Blake Simmons	08630
1	MS9292	Todd Lane	08623
1	MS9292	Benjamin Wu	08634
1	MS9292	Eizadora Yu	08623
1	MS9293	Neal Fornaciari	08530
1	MS9409	Patricia E. Gharagozloo	08365
1	MS9409	Gregory Wagner	08365
1	MS9671	Pamela Lane	08623
1	MS0899	Technical Library	9536
1	MS0359	D. Chavez, LDRD Office	1911


Sandia National Laboratories